Article

First U-Pb (CA-ID-TIMS) Dating of the Uppermost Permian Coal Interval in the Minusinsk Coal Basin (Siberia, Russia) Using Zircon Grains from Volcanic Ashfalls

Vladimir V. Silantiev [1,2,*], Sergey I. Arbuzov [3,4], Marion Tichomirowa [5], Alexandra Käßner [5], Alsu Kh. Izmailova [1], Sergey S. Ilenok [3], Bulat R. Soktoev [3], Nouria G. Nurgalieva [1], Yaroslav M. Gutak [6], Anastasia S. Felker [7], Lyubov G. Porokhovnichenko [8], Nikolai A. Eliseev [2], Veronika V. Zharinova [1], Evgenia M. Nurieva [1] and Milyausha N. Urazaeva [1]

1   Institute of Geology and Petroleum Technology, Kazan (Volga Region) Federal University, 420008 Kazan, Russia
2   Department of Earth Sciences, Branch of the Kazan (Volga Region) Federal University, Jizzakh 130100, Uzbekistan
3   School of Earth Sciences & Engineering, National Research Tomsk Polytechnic University, 634050 Tomsk, Russia; siarbuzov@tpu.ru (S.I.A.)
4   Far East Geological Institute, Far Eastern Branch of the Russian Academy of Sciences, 690022 Vladivostok, Russia
5   Institute of Mineralogy, Technical University Bergakademie Freiberg, 09599 Freiberg, Germany; tichomir@mineral.tu-freiberg.de (M.T.); alexandra.kaessner@mineral.tu-freiberg.de (A.K.)
6   Institute of Mining and Geosystems, Siberian State Industrial University, 654007 Novokuznetsk, Russia
7   Arthropod Laboratory, Borrisiak Palaeontological Institute of the Russian Academy of Sciences, 117647 Moscow, Russia
8   Faculty of Geology and Geography, National Research Tomsk State University, 634050 Tomsk, Russia
*   Correspondence: vladimir.silantiev@kpfu.ru

Abstract: This study presents the first U-Pb (CA-ID-TIMS) radioisotopic dating of zircon grains extracted from tonsteins within the uppermost Permian coal interval of the Minusinsk Coal Basin (Siberia, Russia). Petrographic, structural, and mineralogical analyses confirm the volcanic ash origin of the tonsteins. The parent pyroclastic materials are identified as rhyolite–pantellerite for tonstein I-22 and dacite–rhyodacite for tonstein I-12. Morphological analysis of zircon crystals, along with cathodoluminescence and melt inclusion studies, confirms their volcanic origin and crystallisation temperatures of 700–900 °C. New radioisotopic dates of 261.4 ± 0.7 Ma and 261.3 ± 0.4 Ma clarify the age of the Izykh Formation, enabling its direct correlation with the Capitanian Stage of the International Chronostratigraphic Chart. The results emphasise the possible discontinuity of the coal-bearing succession of Siberian palaeocontinent and highlight the potential for further stratigraphic refinement through continued radioisotopic dating of tonsteins.

Keywords: Siberia; Permian; tonstein; ashfalls; U-PB dating; CA-ID-TIMS; geochronology; biostratigraphy

1. Introduction

Radioisotopic uranium–lead (U-Pb) dating of individual zircon grains by thermal ionisation mass spectrometry with isotope dilution and chemical abrasion (CA-ID-TIMS) is a widely accepted tool for the direct chronological correlation of local stratigraphic units with the International Chronostratigraphic Scheme [1,2]. The application of U-Pb radioisotopic dating is particularly successful in coal-bearing strata, which often contain numerous tonsteins, considered to be altered volcanic ashes originating from tectonic activity and explosive volcanism [3–9].

Radioisotopic uranium–lead (U-Pb) dating has provided a chronostratigraphic framework for the coal basins of Euramerica (North America [10], Western Europe [7,11–14], and

Eastern Europe (Donets Basin) [15,16]), Gondwana (Australia [17–19] and South America [20–25]), and China [26–28]. In recent years, a number of radioisotopic ages from the coal basins of the Siberian palaeocontinent have been published, including data from the Irkutsk Basin [29] and the Kuznetsk Basin [30–32]. In this paper, we continue this series of publications.

The coal-bearing succession of the Minusinsk Coal Basin includes several tonsteins, which have been studied very thoroughly from geochemical viewpoints [33–38]. The increased attention being paid to the Minusinsk Coal Basin tonsteins is due to the accumulations and elevated Zr-Nb-Hf-Ta-REE-Ga concentrations [34,37,38] attributed to volcanic activity [39–43].

The uppermost Permian coal-bearing interval, including two thick (up to 12 m) coal seams, XXX and XXXI, has been identified as the Izykh Formation (Fm) [44]. Tonsteins containing zircon grains, dated by the radioisotopic method, were sampled from the coal seam XXX, located in the middle part of the formation.

As more plant remains and invertebrate fossils were studied from the Izykh Fm, its biostratigraphic age became younger. Initially, it was considered to be Cisuralian, i.e., Asselian–Sakmarian (290–295 Ma) ([45–49] and others) and Artinskian–early Kungurian (280–290 Ma) [50]. Later, it began to be defined as the late Kungurian (about 275 Ma) [51], and more recently as the Roadian (about 270 Ma) [44]. This paper presents radioisotopic evidence that the Izykh Fm is approximately 10 million years younger than previously thought based on biostratigraphic data.

The aim of this paper is to present data on the radioisotopic age of the Permian coal-bearing strata of the Minusinsk Basin, which enables direct correlation with the International Chronostratigraphic Chart.

2. Geological Background

The Minusinsk Coal Basin is one of the late Palaeozoic coal basins of the Altai–Sayan Fold Belt (Figure 1) and is situated in the south part of the Minusinsk intermountain trough, a complex synclinorium extending for almost 300 km from south to north. The Minusinsk intermountain trough borders with the pre-Devonian folds of the Kuznetsk Alatau, the Western Sayan, and the Eastern Sayan; in the north, it is joined with the West Siberian Plate [34,52].

The prevailing view is that the Altai–Sayan Fold Belt was formed as a result of the impact of the Palaeo-Asian oceanic plate and the Siberian palaeocontinent in the Neoproterozoic–Mississippian. The opening and closure of the Palaeo-Asian oceanic plate is considered to be the main driving force of the accretion and collision of different-aged microcontinents, volcanic island arcs, and active and passive margins of microcontinents with each other and with the Siberian palaeocontinent [53–58].

The Minusinsk intermountain trough includes a number of subordinate local depressions and uplifts that are superposed on the Baikalian–Salairian metamorphic fold basement located at a depth of 6000–7000 m. The overlying rocks comprise volcaniclastic, clastic, and coal-bearing strata of the Middle Devonian (Givetian), Carboniferous and Permian, and Mesozoic and Cenozoic deposits [34,52].

The lower boundary of the coal-bearing limnic succession is unconformable and is accepted at the base of a thin conglomerate overlain by coal-bearing shales and coals, dated as Serpukhovian by plant and invertebrate fossils [44–51]. It is assumed that most of the coal-bearing strata of the Minusinsk intermountain trough have been destroyed by post-Mesozoic erosion [52], and the remaining part (1100 to 1800 m thick) is preserved mainly in the south of the trough in several synclines (or muldes) which are referred to as the Minusinsk Coal Basin. The total area of the Minusinsk Coal Basin is 8100 km^2, while the area of commercial coal measures is about 1100 km^2 [52]. The coal-bearing succession includes strata from the late Mississippian to the late Guadalupian (Figure 2).
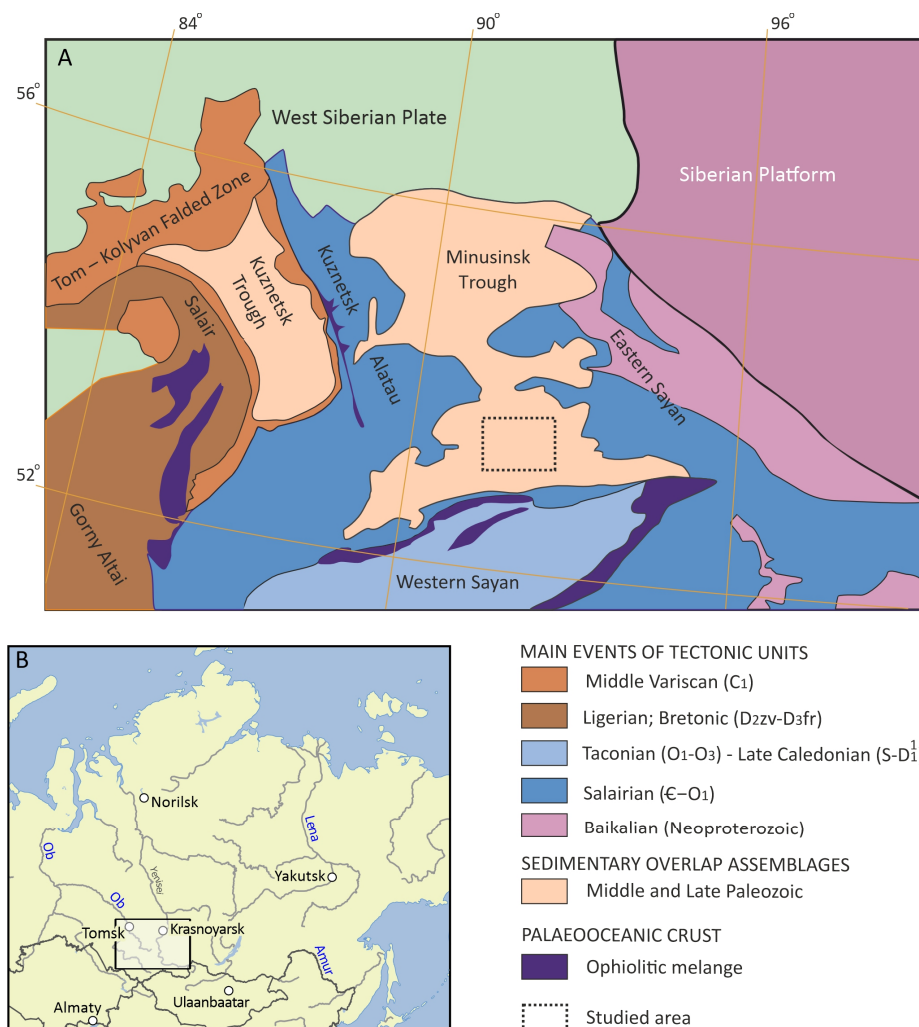
Figure 1. Tectonic scheme (**A**) illustrating the position of the study area within the Altai–Sayan folded region; simplified from [54–56]; (**B**) overview map with outlines of tectonic scheme.

The first stratigraphic scheme of the coal-bearing succession of the Minusinsk Coal Basin and a 1:200,000 scale geological map were developed in the late 1920s. Subsequently, the stratigraphic schemes and geological maps were detailed in the 1940s–1970s. In 1997, Victor Sivtchikov [44] revised the stratigraphic scheme of the coal-bearing succession based on new palaeontological data and a comprehensive summary of all available materials. We adopt this revised scheme in this paper.

The synclines (or muldes) of the Minusinsk Coal Basin are separated from each other by anticlinal folds (Figure 3). The territory we studied is a part of the Izykh Mulde, representing a rounded isometric structure with a flat bottom and sloping (10–30°) sides (Figure 4). The diameter of the mulde along the basement of the Serpukhovian coal-bearing strata is 25 km. The mulde is composed of coal-bearing strata accumulated from the Serpukhovian to the Capitanian.

The coal-bearing strata are composed of siltstones (50%), sandstones (30%), mudstones (10%), and coals (6%); other rocks such as conglomerates, gritstones, and limestones are subordinate. The productive coal deposits of the Minusinsk Basin include 122 coal seams and interbeds, of which 35 are contiguous or split coal seams. Generally, the main coal seams are traceable in all the basin muldes.
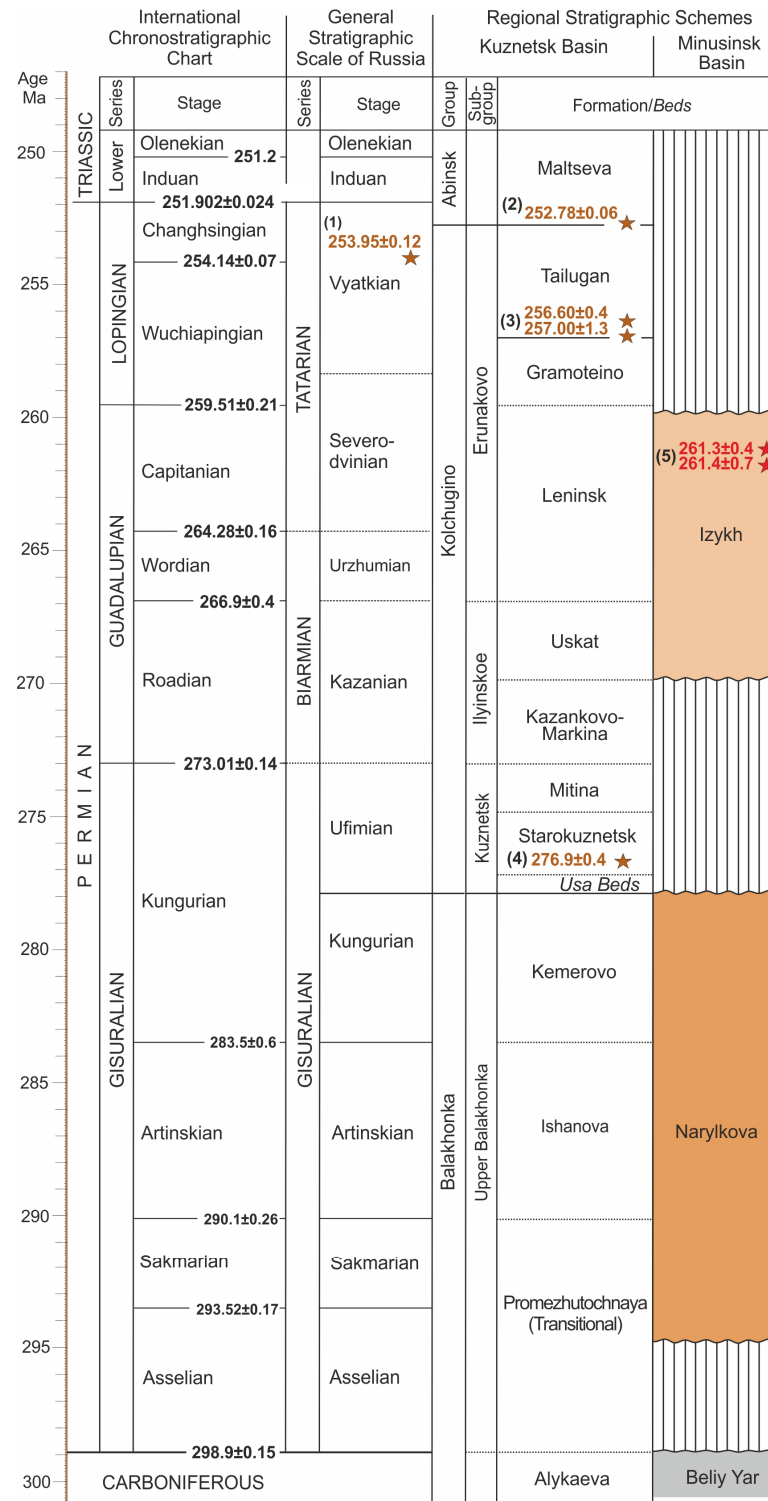
Figure 2. Regional stratigraphic scheme of the Permian of the Minusinsk Coal Basin [59], with modifications based on new radioisotopic datings, correlated with the Regional Scheme of the Kuznetsk Basin [60,61] and compared with the General Stratigraphic Scale of Russia [62] and the International Chronostratigraphic Chart [63]. The radioisotopic datings highlighted with star symbols are based on (1) ref. [64]; (2) ref. [30]; (3) ref. [31]; (4) ref. [32]; and (5) this article.
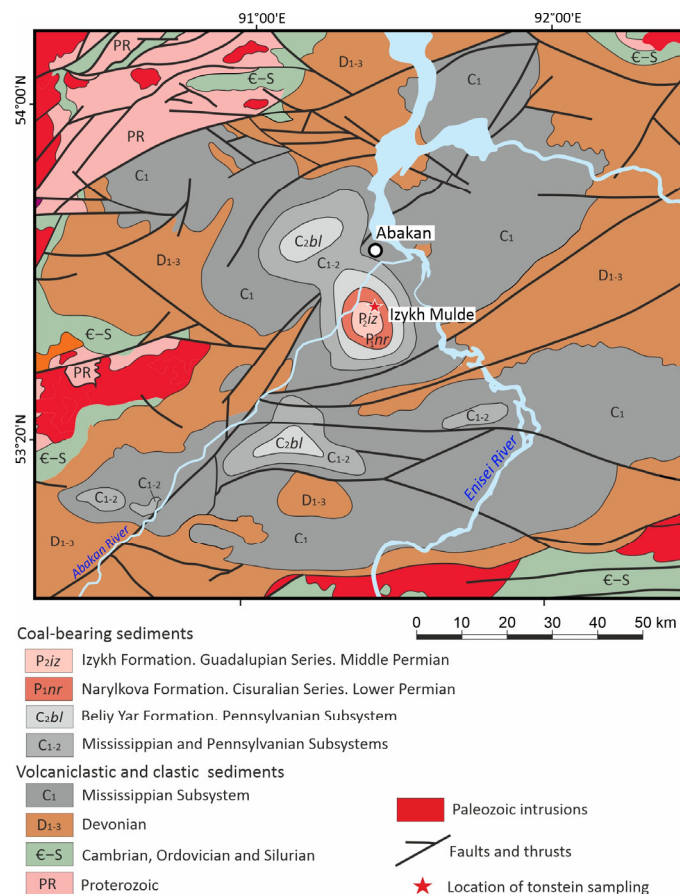
Figure 3. Geological map of the Minusinsk Coal Basin (simplified from [65]) and sampling location within the Izykh syncline (mulde).
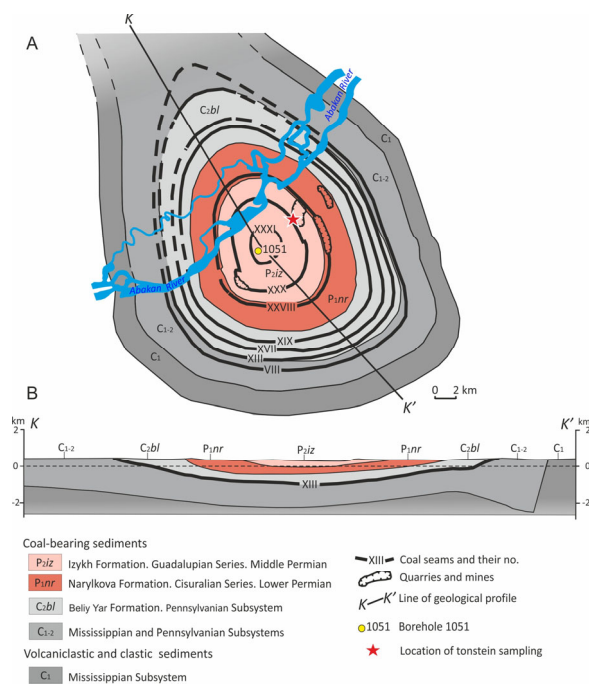
Figure 4. Geological map of the Izykh syncline (mulde) (**A**) and profile on line K–K′ (**B**) (simplified from [52]); sampling location is highlighted with star symbol.

Each syncline (or mulde) of the basin is considered a separate coalfield, with its own index system for coal seams. In particular, the coal seams of the Izykh Mulde are numbered with Roman numerals from I to XXXI. Additional coal seams above the main seam are indexed by the number of the main seam with a letter in upper case (e.g., XV[a], XV[b], etc.). Additional coal seams below the main seam are marked by the main seam number with one or several apostrophes (e.g., XV′, XV″, etc.).

The Izykh Fm, the subject of this article, is distributed only in the central part of the Izykh Mulde (see Figures 3 and 4). The lower boundary of the Fm coincides with the top of coal seam XXVIII. The Izykh Fm overlies the Narylkova Fm with an unconformity (Figure 5) spanning from the upper Kungurian to the lower Roadian (Figure 2).
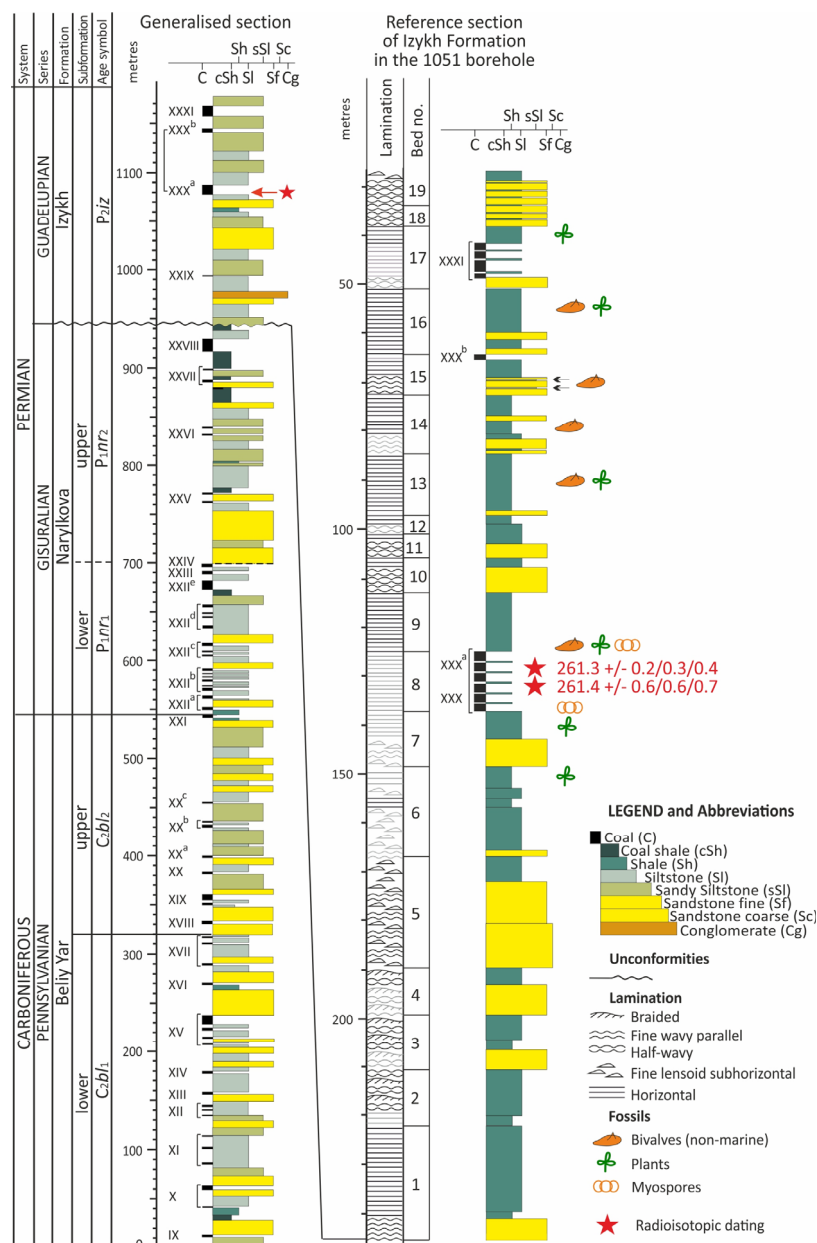
Figure 5. Generalised stratigraphic section of the Pennsylvanian and Permian (Cisuralian and Guadalupian) of the Minusinsk Coal Basin (compiled from [34,52,59]) (A) and the reference section of the Izykh Formation in the 1051 borehole, Izykh Coalfield (compiled by V. M. Yadrenkin in [44]); the star symbols indicate the radioisotopic dating discussed in this article.

The Izykh Fm (250–260 m) is composed predominantly of siltstones (more than 50%), including coal seams, interlayers of shales and sandstones, and subordinate lenses of siderites and conglomerates. The rocks include an admixture of ash material. At 30–35 m above the base of the formation, a surface of erosion and unconformity is established. *The lower part* of the Izykh Fm (140–150 m) is represented by a coal-free interval consisting of siltstones and sandstones with only one thin coal seam (XXIX) and several local interlayers. Further up the section, the number and thickness of sandstone beds increase. *The upper part* of the formation (100–110 m) is composed primarily of fine-grained clastic rocks, including siltstones, shales, and fine sandstones. It also contains two thick coal seams, indexed as XXX and XXXI.

The XXX coal seam (in total 4.0–9.3 m) typically includes five to seven coal beds with a thickness of 0.1 to 6.5 m, separated by rock interlayers with a thickness ranging from 0.3 to 3.0 m. In certain locations, the XXX seam is divided into additional seams, designated as XXX[a] and XXX[b]. The coals of the XXX seam are characterised by their heterogeneity of composition, caused by the interbedding of semi-glossy, matte, and semi-matte coals. The vitrinite reflectance varies between 0.58% and 0.62%, which corresponds to the first stage of coal metamorphism [52]. The XXX seam contains a number of tonsteins (from 1 to 30 cm thick) which were sampled for zircons (see the Materials Section).

The presence of numerous tonsteins is a remarkable feature of the coal seams in the Minusinsk Basin. Their thickness usually varies from a few millimetres to 5 cm [33]. In coal seams, tonsteins usually form packages consisting of several layers located at distances from 5 to 30 cm from each other. The intervals between adjacent packages are up to several metres.

The clastic intervals separating coal seams sometimes also contain single tonsteins, which are associated with thin clayey rocks. In general, tonsteins can be confidently traced over long distances and can be used for correlation. The primary ash material of tonsteins is usually altered to kaolinite, which has been determined by X-ray diffraction analysis [33]. The composition of the primary tuffs is thought to range from andesite to pantellerite. The most common hypothesis for the accumulation of this material is periodic ashfalls that formed successive series (packages) of layers [34].

3. Materials

Samples of tonsteins for zircon extraction were taken in 2015 and 2018 within the Izykh open-cast coal mine from the XXX and XXX[a] seams, which lie just above the middle of the Izykh Fm (Figures 4–6). In the coal seams, tonsteins appear as light-coloured thin continuous layers of siltstone or mudstone traceable for kilometres. Two tonsteins, 1–2 cm thick, were collected (1.5–2.0 kg) from each coal seam (see Figure 7). The fifth tonstein sample was collected from a siltstone parting (0.45 m thick) with increased radioactivity (25 μR/h) separating coal seams XXX and XXX[a]. The tonstein I-12 from seam XXX[a] and the tonstein I-22 from the siltstone parting were the only samples that contained zircon grains in sufficient quantity for radioisotopic dating. In total, approximately 200 zircon grains were extracted from the two tonsteins and analysed with different methods.

Tonsteins are soft clayey rocks that range in colour from light yellowish-grey to greyish-brown (Figure 8). When wet, they take on a darker hue. Some samples display fine secondary subhorizontal foliation (Figure 8A).

The zircons extracted from tonsteins I-12 and I-22 show no visible features of transportation or roundness (Figure 9).

Figure 6. Outcrop of the upper part of the Izykh Fm in the Izykh coal mine showing the location of tonstein sampling.
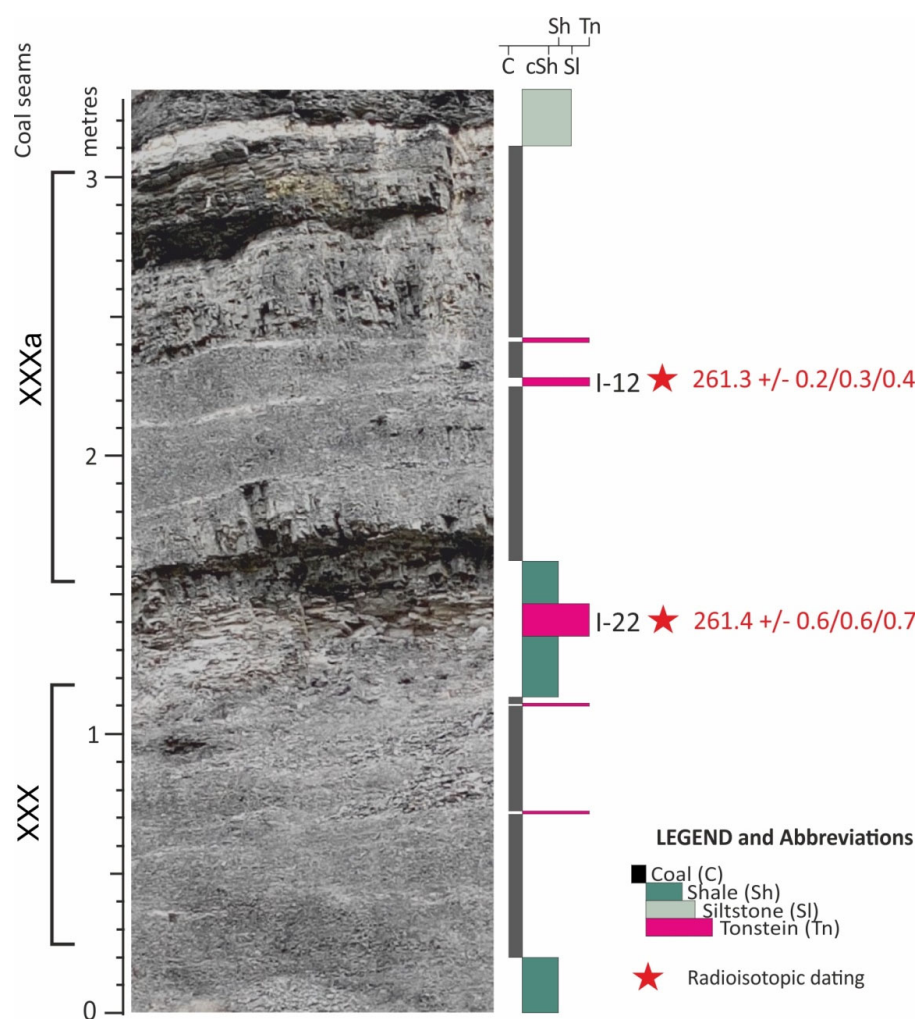
Figure 7. Location of tonsteins I-12 and I-22 in coal seams XXXa and XXX.
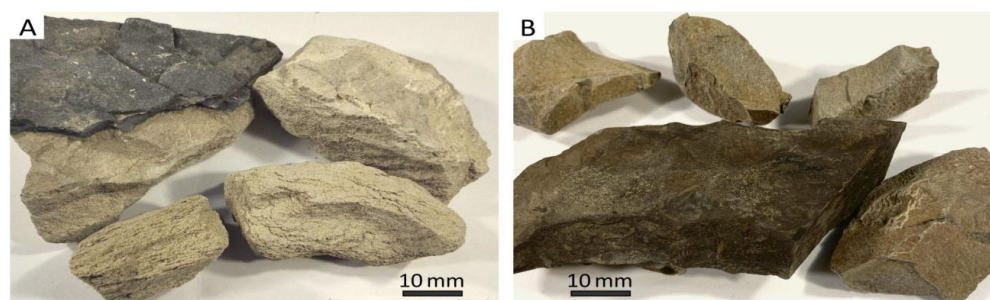
Figure 8. Tonstein samples from the coal seams XXXa and XXX: (**A**) tonstein I-12; the upper left sample retained contact with the adjacent coal, and (**B**) tonstein I-22; the darker sample is wet.
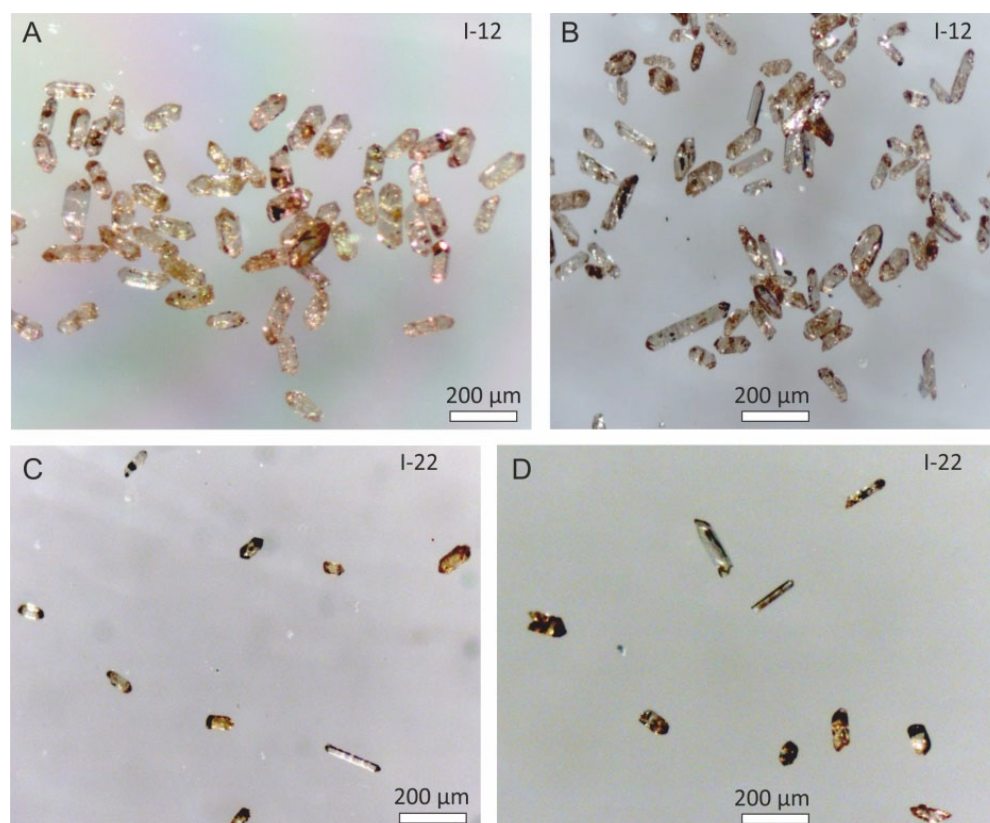
Figure 9. Zircon grains extracted from tonsteins I-12 (**A,B**) and I-22 (**C,D**).

4. Methods

X-ray diffraction analysis was conducted in the Laboratory of Lithology of the Tomsk Scientific Research and Design Institute of Oil and Gas using the RIGAKU ULTIMA IV X-ray diffractometer (Tokyo, Japan) with the integration of X-ray film imaging in Bragg–Brentano geometry (performed by B.R. Soktoev). The following parameters were used for the diffraction patterns: Cu anode, X-ray tube voltage of 40 kV, current of 30 mA, power of 1.2 kW, imaging speed of 1°/min, pitch of 0.02°, and imaging angles of 2Θ from 5° to 70°. To improve the quality of XRD and facilitate the identification of low-content minerals, specific sample processing techniques were employed [66]. A Rietveld XRD analysis was conducted using Siroquant v5 software (Siroquant, Mitchell, Australia) [67] to perform quantitative mineralogical calculations on the whole-rock data [68].

Electron microscopy and X-ray energy-dispersive spectrometry of tonsteins was performed at the International Innovative Scientific and Educational Centre "Uranium Geology" of the Engineering School of Natural Resources of the National Research Tomsk Polytechnic University on a Hitachi S-3400N scanning electron microscope (Tokyo, Japan)

equipped with a Bruker X@Flash 5010 X-ray energy-dispersive spectrometer (Berlin, Germany). The study of the samples was carried out in low vacuum mode, using backscattered electrons.

Inductively coupled plasma mass spectrometry (ICP-MS) was employed to analyse the elemental composition of tonsteins using the iCAP Qc equipment (ThermoFisher Scientific, Bremen, Germany) at the Institute of Geology and Petroleum Technologies of Kazan Federal University. The standard sample preparation process was carried out using the Ethos Up microwave decomposition oven (Milestone, Italy). The prepared solution was analysed on a mass spectrometer that had been calibrated with multi-element standards at concentrations ranging from 1 to 100 ppb for each element. The resulting values were then recalculated to the initial concentration, taking into account the blank sample, suspension, and dilution of the solution.

Analysis of the Morphological Features of Zircon Crystals. The aim of this study was to verify the volcanogenic origin of zircon crystals (zirconium orthosilicate, $Zr(SiO_4)$) extracted from tonsteins. As is widely recognised, zircon crystallises in a tetragonal syngony. Additionally, zirconium is frequently isomorphically substituted by uranium, thorium, and other radioactive elements. The zirconium crystal lattice is highly susceptible to changes in the chemical composition of the growth medium and the crystallisation temperature. Variations in these parameters result in the crystallisation of different morphotypes, including short prismatic, isometric, and needle-like crystals [69].

The morphology of zircon crystals was studied in accordance with the approach proposed by J. Pupin [70], utilising the diagram he devised (Figure 10), which correlates the shape of crystals with the crystallisation temperature. The study of morphology focused on three key areas: (a) habitus, which determines the dominant simple crystallographic form; (b) the perfection of the crystal facets or the degree of idiomorphism; and (c) the character of facets, including the presence of combinational hatching, deformation, abrasion, signs of dissolution, and secondary recrystallisation.
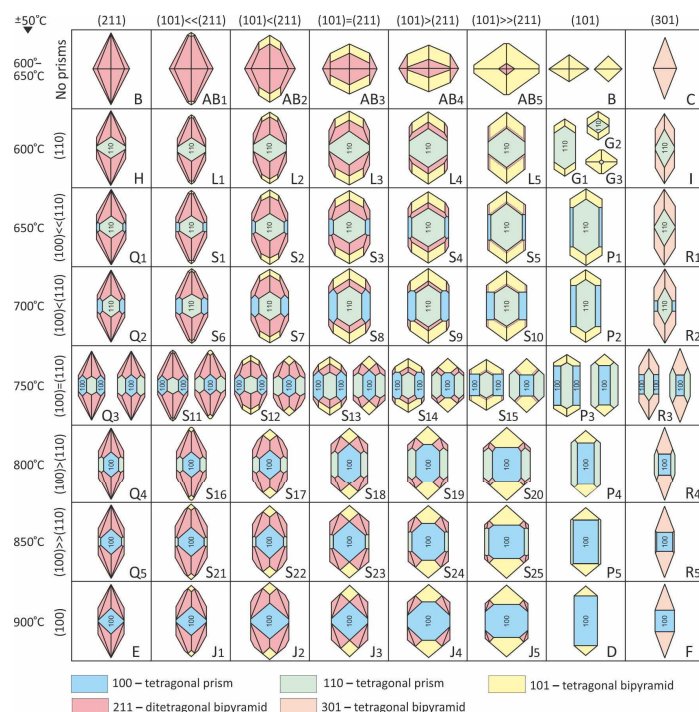

Figure 10. Main types and subtypes of zircon crystals and the corresponding geothermometric scale according to J.P. Pupin [70]. The letter designations of crystal types and subtypes are provided in accordance with the classification system of J.P. Pupin (p. 209, Table 1 in [65]).

Table 1. Mineral composition of the studied tonsteins, %.

Mineral	Tonstein I-12	Tonstein I-22
Kaolinite	42.6	56.2
Quartz	35.0	22.9
K-feldspar (sanidine and microcline)	9.8	12.5
Albite	4.2	5.6
Apatite	11.7	2.7
Total	99.1	99.9

Scanning electron microscope images of zircon grains (over 150) were obtained at the Institute of Geology of the Technical University of Freiberg Mining Academy using a JEOL JSM-7001F Field Emission Scanning Electron Microscope (Freising, Germany).

Cathodoluminescence was applied to study the internal structure of zircon crystals and to select homogeneous crystals for radioisotopic dating. Heterogeneous zircons characterised by the presence of ancient cores and young facets were not used for dating. Sample preparation of zircon grains for cathodoluminescence was carried out using epoxy resin, abrasives (10, 5, and 1 micron), and the Struers RotoPol 35 grinding equipment (Struers GmbH, Willich-Schiefbahn, Germany). Cathodoluminescence photography (more than 150 images) was carried out at the Institute of Geology of the Technical University of Freiberg Mining Academy on a JEOL JSM-7001F microscope.

The study of melt inclusions in zircon grains (5 grains from each tonstein sample) was carried out at Kazan Federal University, Institute of Geology and Oil and Gas Technologies, using Linkam THMS600 (Salfords, UK) with an operating temperature range from $-196\,°C$ to $600\,°C$.

Radioisotopic dating methods. Tonstein samples were processed at the Kazan Federal University. The most promising zircon grains were then sent to the Isotopic Laboratory, Institute of Mineralogy, Technische Universität Bergakademie Freiberg (Freiberg, Germany) for precise dating using CA-ID-TIMS.

Zircon extraction. Zircons were extracted from the tonsteins using three standard procedures involving dimethyl sulfoxide ($(CH_3)_2SO$), ultrasonic dispersion, and heavy liquid GPS-V (a concentrated aqueous solution of sodium heteropolytungstate) (for details, see [32]).

Zircon Dating by Chemical Abrasion–Isotope Dilution–Thermal Ionisation Mass Spectrometry. Selected zircon grains (ca. 30–50 grains with the most idiomorphic forms) were annealed at $900\,°C$ for 96 h and then chemically abraded at $210\,°C$ for 12 h (sample I-22) and 14 h (sample I-12) with concentrated HF and HNO_3 in a pressurised Parr dissolution vessel. This procedure dissolves crystal domains suspected of post-crystallisation lead loss by causing severe radiation damage [71].

The acid was then completely pipetted out together with the dissolved zircon material and 3.5 N HNO_3 was added to the remaining zircon grains and fragments and left for 30 min at $50\,°C$ to remove surface lead. Several cleaning cycles with water combined with repeated ultrasonic treatment were carried out before individual zircon fragments were selected for further processing. Individual zircon grains/fragments were washed with 3.5 N HNO_3 and transferred into clean microcapsules with a small drop of this liquid and four drops of concentrated HF. Samples were spiked with a ^{205}Pb-^{233}U-^{235}U- tracer solution (ET535 at TU Bergakademie Freiberg) [72]. For final dissolution, the microcapsules were placed in pressurised Parr dissolution vessels and heated to $200\,°C$ for 48 h, followed by drying at $130\,°C$ and then redissolving in 6 N HCl for 24 h at $200\,°C$ to convert to chlorides. After repeated drying, the samples were dissolved in ten drops of 3.1 N HNO_3 and transferred into microcolumns for column chemistry. The U and Pb were separated from the rest of the sample by anion exchange chromatography using HCl and H_2O. The U- and Pb-containing fraction was applied to pre-degassed rhenium filaments with a drop of

silica gel [73] and measured on an IsotopX Phoenix Mass Spectrometer using a SEM Daly ion counter (IsotopX, Middlewich, UK).

The accuracy of the dating results was checked by repeated measurements of the zircon standards 91500 [74] and Temora 2 [75]. The published ages of Temora 2 were determined as 416.8 ± 0.3 Ma [75] and 417.35 ± 0.05 Ma [76]. Our date of 417.5 ± 0.5 Ma (Figure 17, Supplementary Materials, Table S1) is in perfect agreement with these values. Our weighted mean ^{206}Pb/^{238}U age of 1064.1 ± 1.3 Ma is within the accepted values of 1062.4 ± 0.4 Ma [74] or 1063.6 ± 0.3 Ma [77]. Based on the standard dating results, we consider the present CA-ID-TIMS ages to be accurate at the 0.1% level.

5. Results

Petrography of tonsteins. An analysis of the structural features and mineralogical composition of tonsteins was conducted with a petrographic microscope. The tonsteins represent a silty-clayey rock devoid of primary lamination (see Figure 11). The main mass of the rock is composed of kaolinite, including clusters and phenocrysts of organic matter. Kaolinite is represented by a range of forms, including cryptocrystalline mass, individual crystals, aggregates of crystals, and pseudomorphoses on feldspars and mica. The significant organic matter content is confirmed by the rather high Loss on Ignition (LOI) values of 35.6 (tonstein I-12) and 13.6 (tonstein I-22) (Table 1). The silty-clayey mass comprises a large number of angular crystals and grains of quartz and feldspar. The lack of lamination is further evidenced by the non-oriented arrangement of mineral grains, crystal aggregates, and clots of organic matter (Figure 11A,B).
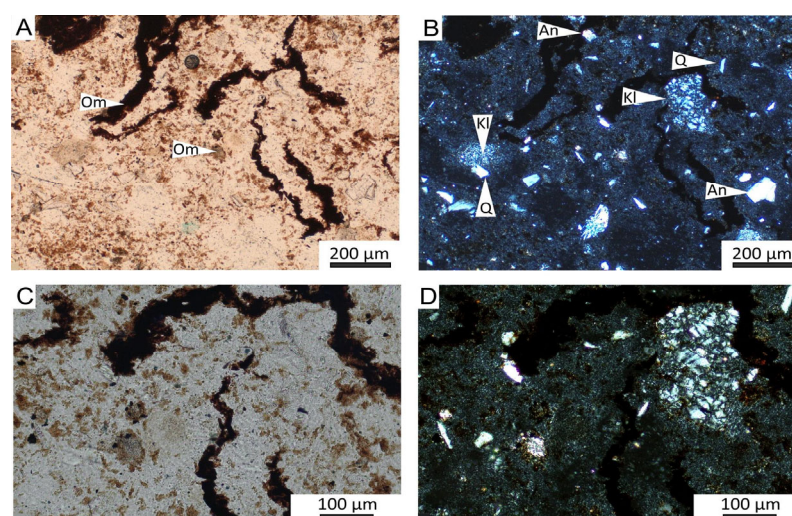
Figure 11. Tonstein structure in thin section: (**A**)—homogeneous cryptocrystalline mass of kaolinite with clusters and phenocrysts of organic matter (Om); (**B**)—the same in crossed nicols: An—anorthoclase; Kl—aggregates of kaolinite crystals; Q—quartz; (**C,D**)—the same section in higher magnification; (**D**)—in crossed nicols. Tonstein I-12.

X-ray diffraction (XRD) analysis. Tonsteins are predominantly composed of kaolinite (42.5–56.2%) and quartz (22.9–35.0%) (Table 1), with subordinate contents of K-feldspars (sanidine and microcline) (9.8–12.5%), albite (4.2–5.6%), and apatite (2.7–11.8%).

Scanning electron microscopy/energy-dispersive X-ray spectrometry (SEM-EDS) of tonsteins enables the detection and identification of sparsely distributed and accessory mineral phases and significantly complements the list of minerals established by XRD analysis.

Tonstein I-12 contains, in addition to the minerals listed in Table 1, sphalerite, celestine, barite, fluoroapatite, brass with lead nugget inclusions, illite, ilmenite (pseudorutile), and baddeleyite.

Tonstein I-22 contains, in addition to the minerals listed in Table 1, zinc nuggets, sphalerite, pyrite, pyrite with nickel admixture, montmorillonite, anorthoclase, barite, and

celestine. According to previous studies [38], tonstein I-22 also includes Zr-bearing minerals represented by zircon, baddeleyite, and complex Ca-Nb-Zr-P silicates of variable composition, as well as lanthanides (monazite) and nodular sulphides (galena and sphalerite).

Major elements of tonsteins determined by inductively coupled plasma atomic emission spectroscopy (ICP-AES). The content of rock-forming oxides in tonsteins I-12 and I-22 and their average composition in post-Archean upper continental crust (UCC) [78] and shales [79] are summarised in Table 2.

Table 2. Content of major element oxides in the studied tonsteins determined by ICP-AES [38].

Major Element Oxides (Weight %)	Tonstein I-12	Tonstein I-22	UCC	NASC
SiO_2	34.7	49.8	66.6	64.8
TiO_2	0.59	0.65	0.64	0.70
Al_2O_3	16.4	27.8	15.4	16.9
Fe_2O_3	0.81	0.86	5.61	6.30
MnO	0.011	0.006	0.10	0.06
CaO	3.61	1.58	3.59	3.63
MgO	0.20	0.31	2.48	2.86
K_2O	0.85	0.71	2.80	3.97
Na_2O	0.18	0.37	3.27	1.14
P_2O_5	2.16	0.88	0.15	0.13
Loss on Ignition (LOI, %)	35.6	13.6	-	-
Total	99.7	99.8	100.64	100.49
SiO_2/Al_2O_3	2.12	1.79	4.3	3.8
TiO_2/Al_2O_3	0.036	0.023	0.042	0.041

Note. All oxide values are in weight %. Average chemical composition: UCC—upper continental crust, post-Archean [78], NASC—North American Shale Composite [79]; the orange colour indicates increased values while the blue colour indicates decreased values; values close to the average content are not coloured.

Tonstein I-12 has TiO_2, Al_2O_3, and CaO contents close to the average chemical composition, with the exception of P_2O_5, which is more than an order of magnitude higher. The contents of the other major element oxides are lower than the average values: SiO_2 is approximately half the average, and Fe_2O_3, MnO, MgO, K_2O, and Na_2O are almost an order of magnitude lower. Tonstein I-22 has elevated values of Al_2O_3 and P_2O_5, while the TiO_2 content is close to the average composition values. The contents of other major element oxides are lower than the average composition values.

The low contents of most rock-forming oxides in the studied tonstein samples are associated with LOI (Loss on Ignition), due to the presence of organic matter. Upon recalculating the data for inorganic matter, it is evident that the tonsteins are enriched in TiO_2, Al_2O_3, CaO, and P_2O_5. The increase in alumina and titanium oxide concentrations is attributed to the loss of the elements, particularly of silica, potassium, and sodium, which occurred during the transformation of the parent ash material into tonstein. The concentrations of CaO and P_2O_5 are associated with the presence of stable fluorapatite in the source material. The recalculated content of rock-forming oxides aligns well with the mineral composition shown in Table 1. The reduced contents of most rock-forming oxides suggest that the tonsteins, derived from volcanic ash material, are geochemically distinct from basin sedimentary rocks, which predominantly consist of clastic material supplied from source areas.

The SiO_2/Al_2O_3 ratio in the studied tonsteins ranges from 1.79 (tonstein I-22) to 2.12 (tonstein I-12), and the $TiO_2/Al2O_3$ ratio from 0.036 (tonstein I-22) to 0.023 (tonstein I-12). These values are lower than these ratios for average chemical composition. The lower SiO_2/Al_2O_3 ratio compared to the average chemical composition indicates silica removal during ash kaolinisation, and the lower TiO_2/Al_2O_3 ratio indicates the acid (rhyodacite) composition of the primary ashes [4].

Trace elements of tonsteins obtained by the ICP-MS method. The contents of trace elements in the studied tonsteins, the average contents in sedimentary rocks [80,81], in the post-Archean upper continental crust (UCC) [78], in acid volcanic rocks [80,81], and in coal ashes [82] are summarised in Table 3.

Table 3. Trace elements (ppm) in the studied tonsteins and average concentrations in relevant rocks.

Element	Tonstein I-12	Tonstein I-22	Sedimentary Rocks [1]	Upper Continental Crust (UCC) [2]	Acid Volcanic Rocks [3]	Coal Ashes [4]
Li	68.2	20.7	33	21	26	66
Be	4.3	0.45	1.9	2.1	4	9.4
Sc	11.4	6.9	9.6	14	4.2	23
V	8.4	11.9	91	97	60	155
Cr	2.4	3.4	58	92	8.5	100
Co	1.3	1.7	14	17.3	4.8	32
Ni	21.9	92.2	37	47	8	76
Cu	68.6	57.5	31	28	15	92
Zn	100.4	55.7	43	67	35	140
Ga	20.8	36.2	12	17.5	26	33
Ge	9.2	14.9	1.4	–	1	15
As	14.9	10.8	7.6	–	4.3	47
Se	6.4	8.1	0.27	–	0.093	8.8
Rb	14.6	8.4	94	84	190	79
Sr	236	218	270	320	240	740
Y	81.2	39.2	29	21	24	51
Zr	94.8	115.3	170	193	110	210
Nb	7.1	4.6	7.6	12	26	20
Mo	1.4	1.2	1.5	–	3.4	14
Cd	0.3	0.2	0.8	0.09	0.3	1.2
Sn	2.1	3.0	2.9	2.1	3.5	6.4
Sb	0.1	0.70	1.2	0.4	–	6.3
Cs	0.6	0.9	7.7	4.9	10	6.6
Ba	445	231	410	628	480	940
La	35.6	88.1	32	31	31	69
Ce	76.9	169.8	52	63	58	130
Pr	8.7	16.7	6.8	7.1	10	20
Nd	35.5	62.0	24	27	27	67
Sm	7.9	10.8	5.5	4.70	5.2	13
Eu	1.8	1.6	0.94	1.0	1.5	2.5
Gd	8.6	9.8	4	4.0	5	16
Tb	1.3	1.4	0.69	0.70	0.82	2.1
Dy	8.8	7.4	3.6	3.90	6	14
Ho	2.1	1.4	0.92	0.83	1.7	4.0
Er	7.3	3.4	1.7	2.30	3.6	5.5
Tm	1.1	0.5	0.78	0.30	1	2.0
Yb	8.0	3.0	2.0	1.96	2.5	6.2
Lu	1.1	0.4	0.44	0.31	0.55	1.2
Hf	3.9	5.2	3.9	5.3	4.1	8.3
Ta	0.9	1.9	1.0	0.9	1.8	1.7

Table 3. *Cont.*

Element	Tonstein I-12	Tonstein I-22	Sedimentary Rocks [1]	Upper Continental Crust (UCC) [2]	Acid Volcanic Rocks [3]	Coal Ashes [4]
W	0.5	0.3	2.0	–	1.4	6.9
Tl	0.13	0.07	0.89	0.9	2.1	4.9
Pb	19.7	30.0	12	17	23	47
Th	12.3	31.9	7.7	10.5	13	21
U	3.8	7.1	3.4	2.7	4.5	16
Th/U	3.2	4.5	2.26	3.9	2.9	1.3

Note. All values are in ppm. Average trace element content: [1,3]—ref. [80,81]; [2]—ref. [78]; [4]—ref. [82]; the orange colour indicates increased values while the blue colour indicates decreased values; values close to the average content are not coloured. It should be noted that the values in Table 3 are given for the original samples without LOI. If the correction coefficients are introduced, then all values indicated for tonstein I-12 increase by a factor of 1.55, and for tonstein I-22 by a factor of 1.16. This increase does not affect the results discussed herein.

Tonstein I-12 contains elevated concentrations of Li, Be, Cu, Zn, Ga, Ge, As, Se, Y, Ce, Nd, Sm, Eu, Gd, Tb, Dy, Ho, Er, Tm, Yb, Lu, and Th compared to the average composition of sedimentary rocks and UCC. Conversely, this tonstein shows reduced contents of V, Cr, Co, Ni, Rb, Zr, Cs, W, and Tl. The concentrations of Sc, Sr, Nb, Mo, Cd, Sn, Sb, Ba, Hf, Ta, and U are close to the average values for sedimentary rocks and UCC.

Tonstein I-22 contains elevated concentrations of Ni, Cu, Zn, Ga, Ge, As, Se, Y, La, Ce, Pr, Nd, Sm, Eu, Gd, Tb, Dy, Ho, Er, Yb, Hf, Ta, Pb, Th, and U. Reduced contents are noted for Li, Be, V, Cr, Co, Rb, Zr, Cs, Ba, Tm, W, and Tl. The concentrations of Sc, Sr, Nb, Mo, Cd, Sn, Sb, and Lu are close to the average values for sedimentary rocks and UCC.

The values of some elements recorded in tonsteins I-12 and I-22, both elevated (Be, Ga, Eu, Dy, Er, Tm, Ta, Th) and reduced (Li, V, Cr, Co, Ni, Zr), correlate with the average contents in acid volcanic rocks. Elevated values of elements such as Li, Ni, Cu, Ga, Ge, Se, Y, REE, Hf, Ta, Pb, Th, and U also correlate with concentrations of these elements in coal ash.

General Description of Zircon Crystals. The study of zircon grain populations from tonstein I-22 (60 grains) and tonstein I-12 (100 grains) using optical and scanning electron microscopes revealed in both cases the predominance of medium prismatic crystals (60% and 45%, respectively), with length-to-width ratios ranging from 2 to 4. Short prismatic crystals, with length-to-width ratios less than 2, are subdominant, accounting for 30% and 35%, respectively. Long prismatic crystals, with a length-to-width ratio greater than 4, account for 10% and 20%, respectively. Most grains (about 85%) have well-developed {101}–{211} pyramids. Photographs of crystal populations and individual grains are shown in Figures 9, 12 and 13.

Transparent crystals predominate (more than 55%) in both tonsteins I-22 and I-12. They are either colourless (about 25%) or have yellowish (about 15%) or brownish (about 15%) shades. Opaque muddy crystals account for 45% and are mostly coloured in yellowish and brownish shades; opaque colourless crystals are very rare (2%). In general, zircon grain populations from tonsteins I-22 and I-12 contain approximately 75% idiomorphic grains of good preservation. Rounded grains account for 4–5%, grains with broken edges and faces account for 5–6%, grains with intense fracturing account for about 10%, and finally at least 5% of the grains contain well-defined inclusions.

Morphological Features of Zircon Crystals. Zircon grains from tonsteins I-22 (60 grains) and I-12 (100 grains) were subdivided into main types and secondary subtypes according to the methodological approach of Pupin [70] and the resulting data are shown in Figures 14 and 15.
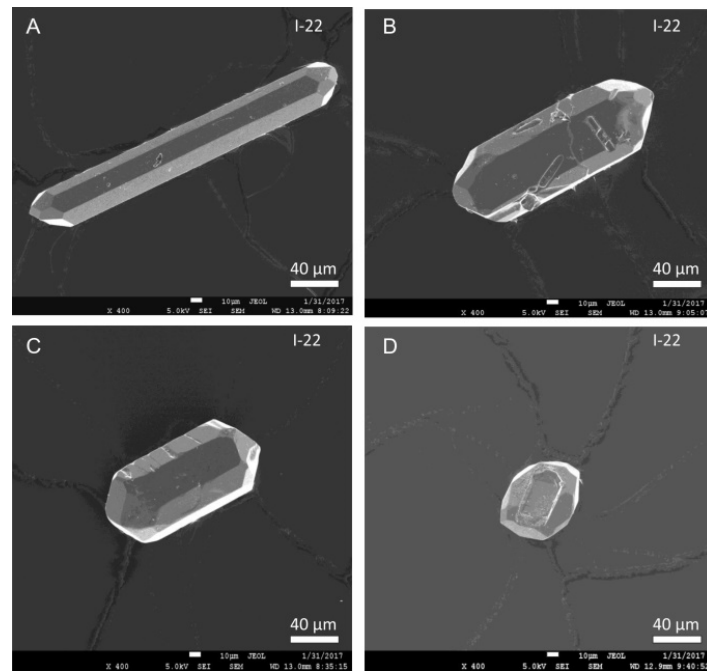
Figure 12. Zircon grains from tonstein I-22: (**A**)—long prismatic crystal; (**B**)—medium prismatic crystal; (**C**)—short prismatic crystal; (**D**)—short prismatic grain; SEM photos.
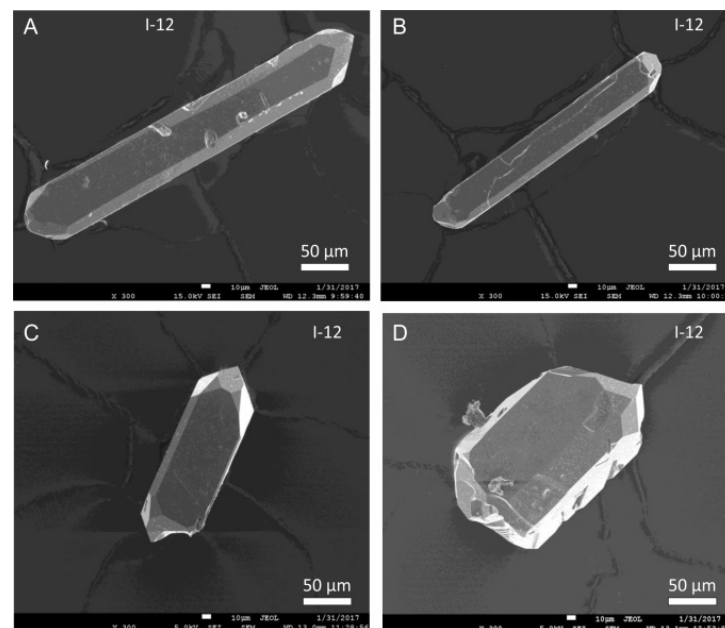

Figure 13. Zircon grains from tonstein I-12: (**A,B**)—long prismatic crystals; (**C**)—medium prismatic crystal; (**D**)—broken crystal; SEM photos.

In tonstein I-22 (Figure 14), the most prevalent zircon grains represent the main type S ({100}–{110} prisms, {101}–{211} pyramids), among which subtypes S_{17} and S_{18} dominate (about 55%), while subtypes S_{23} and S_{25} subdominate (in total about 25%), and the number of other subtypes is of minor value. Scattered grains of the subtype P_5 ({100}–{110} prisms, {101} pyramids) and subtypes Q_4 and Q_5 ({100}–{110} prisms, {211} pyramids) are also recorded.

Figure 14. Quantitative distribution of zircon grain morphotypes from tonstein I-22 according to the diagram of Pupin [70]; morphotypes S17 and S18 with developed prismatic facets {100} predominate.

In tonstein I-12 (Figure 15), the same main types P, Q, and S, as in tonstein I-22, occur. Subtypes S_{18} and S_{19} (about 60%) are dominant; subtype S_{17} (about 15%) and subtypes P_4, Q_4, and S_{20} (in total about 20%) are subdominant; while the remaining six subtypes (Q_2, Q_3, S_9, S_{12}, S_{14}, P_5) are represented by single grains.
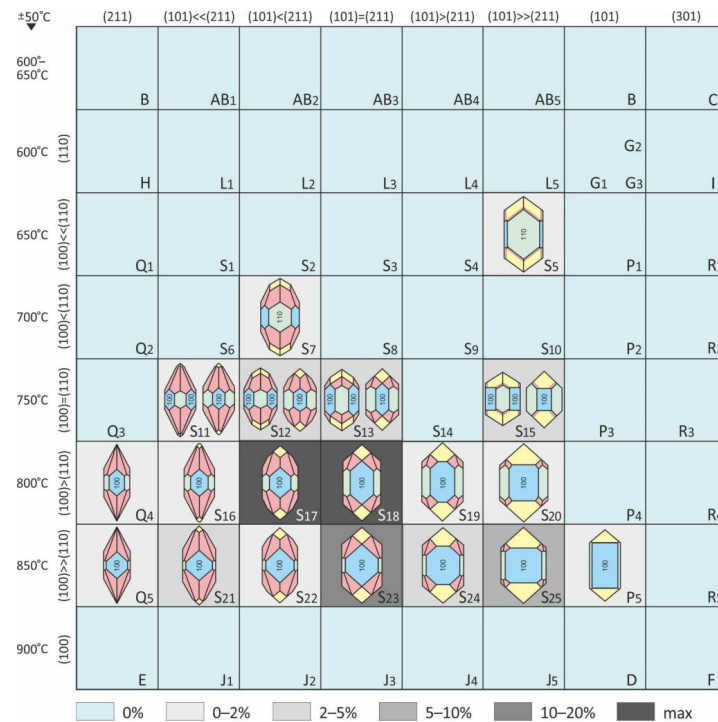

Figure 15. Quantitative distribution of zircon grain morphotypes from tonstein I-12 according to the diagram of Pupin [70]; morphotypes S18 and S19 with developed prismatic facets {100} predominate.

In general, both tonsteins contain crystals of the main types P, Q, and S, among which the subtypes S_{17}, S_{18}, and S_{19} dominate. The morphological subtypes are grouped in the lower part of the diagram [70], suggesting that the crystallisation conditions of most crystals were similar.

The Results of the Cathodoluminescence Study revealed that most of the zircon grains extracted from tonsteins I-22 and I-12 have complex zonality, both parallel-symmetric and asymmetric. Analysis of the cathodoluminescence images enabled us to exclude grains with mechanical disturbances and asymmetric zonality from radioisotope dating, as these features indicate the probable occurrence of an older crystalline core.

Study of Melt Inclusions. Examination of the internal structures of zircon grains extracted from tonsteins I-22 and I-12 indicates the presence of crystalline, vitreous, and gas–fluid melt inclusions (Figure 16) (personal communication, Anatoliy G. Nikolaev, Kazan Federal University). The presence of melt inclusions with gaseous phase indicates the rapid cooling of the primary crystal growth medium and is consistent with geochemical data on the accumulation of tonsteins from volcanic ashfalls.
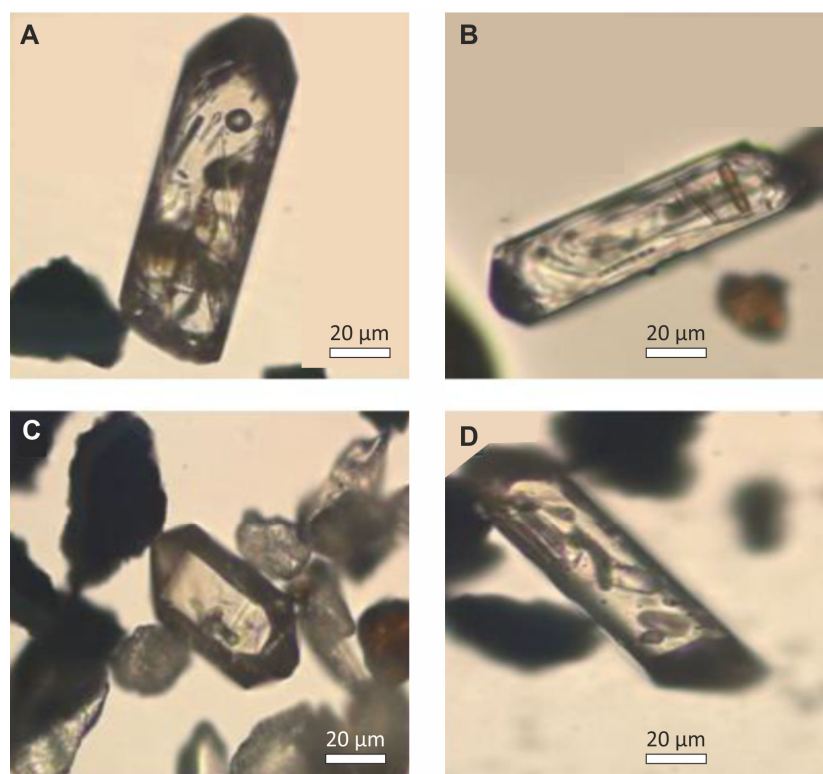

Figure 16. Zircon grains with melt inclusions: (**A**)—crystal containing melt inclusions with gaseous phase, indicating rapid cooling of the primary crystal growth medium; (**B**)—crystal containing crystalline inclusion; well-defined zonality of the crystal is visible; (**C**)—crystal containing vitreous inclusion; (**D**)—crystal containing vitreous and gas–fluid melt inclusions; (**A,B**)—grains from tonstein I-12; (**C,D**)—grains from tonstein I-22.

Analysis of melt inclusions in zircons extracted from the tonsteins I-22 and I-12 indicates a crystallisation temperature range of 700–900 °C, which is in general agreement with the results of the morphological study of zircon crystals.

Results of Radioisotopic Dating. The zircon U-Pb CA-ID-TIMS isotopic results are shown as $^{206}Pb/^{238}U$ ranked age plots in Figure 17 and Annex 1. Mean sample ages representing crystallisation were calculated from established age clusters with the software ET Redux [83]. The error of the weighted mean ages is given as $\pm x/y/z$, where x is the internal 2σ measurement error; y is the internal 2σ error plus tracer calibration uncertainty; and z additionally includes the uncertainty of the decay constant. For discussions, we use the z-error, which includes the internal 2σ measurement error, the tracer calibration uncertainty, and the uncertainty of the decay constant and enables comparison with other dating methods.
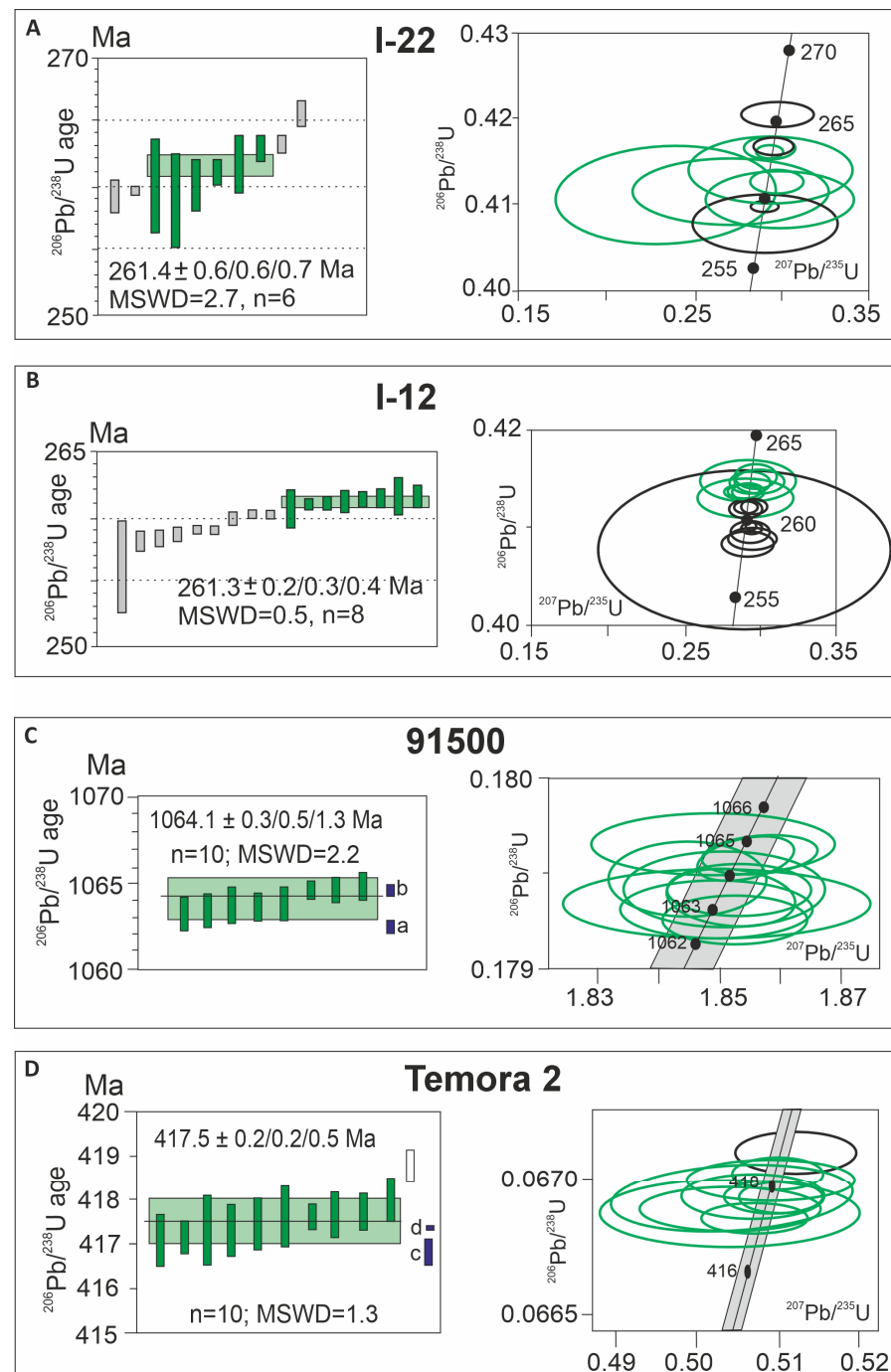
Figure 17. Single-zircon-grain U-Pb CA-ID-TIMS analyses as ^{206}Pb/^{238}U weighted mean dates (left column) and in Concordia diagrams (right column) for both samples, I-22 (**A**) and I-12 (**B**), and two secondary standards, 91500 (**C**) and Temora 2 (**D**), that were dated parallel to the unknowns. In the weighted mean diagrams, each vertical bar represents a single-zircon-grain analysis, including its 2σ analytical (internal) uncertainties; the grey bars were not included in the weighted mean calculation. Vertical green boxes represent the weighted mean age with z—uncertainty. The uncertainty of the weighted mean CA-ID-TIMS dates is reported as ± x/y/z, with x—2σ internal, y—2σ external uncertainty including tracer calibration and z—2σ external uncertainty including ^{238}U decay constant uncertainty [77]. Blue bars for the two standard zircons represent published ages and their uncertainties (a—[74]; b—[77]; c—[75]; d—[76]). In the Concordia diagrams, green ellipses correspond to dates that were chosen for the calculation of the ^{206}Pb/^{238}U weighted mean age; the black ellipses were discarded.

For the sample from tonstein I-22, 10 zircon fragments were dated. The single zircon ages vary from 258.1 to 265.5 Ma and often have a high measurement error due to the small size of the remaining zircon fragments. Six measurements form a cluster with similar ages between 259.8 and 262.8 Ma. These measurements were used to calculate a weighted mean age of 261.4 ± 0.7 Ma (MSWD = 2.7). Two other zircon fragments show older ages, which represent inherited components (e.g., xenocrystic cores), whereas two younger ages represent slight Pb loss.

For the sample from tonstein I-12, we dated 17 zircon fragments. The single zircon ages vary from 257.1 to 261.7. Eight measurements form a cluster with similar ages between 260.7 and 261.7 Ma. These measurements were used to calculate a weighted mean age of 261.3 ± 0.4 Ma (MSWD = 0.5). All other zircon fragments show younger ages, which represent slight Pb loss.

6. Discussion

Petrography of tonsteins. Tonsteins, consisting mainly of cryptocrystalline and re-crystallised kaolinite, and its pseudomorphs after other minerals, are widely known from coal-bearing basins of different ages [3,4,84–88]. The formation of kaolinite is thought to be due to its diagenetic mineralisation from parent volcanic ashfalls under acidic conditions caused by the accumulation and humification of thick peats [89]. The significant amount of organic matter indicates that the burial of the primary sediment, which captured organic matter, occurred rapidly enough and under conditions where biota could not destroy it. The rapid accumulation of matter is confirmed by the presence of angular crystals of quartz and feldspar, as well as by the absence of rock lamination and the unoriented arrangement of mineral grains.

X-ray diffraction (XRD) and scanning electron microscopy/energy-dispersive X-ray spectrometry (SEM-EDS) confirm the mineral composition of the tonsteins established by petrographic studies. The alkaline feldspars, sanidine, albite, and anorthoclase, are considered relict minerals of primary volcanic ash. Sanidine ($K(AlSi_3O_8)$), the highest-temperature (650–800 °C and above) potassium feldspar, is a typical mineral of intermediate-to-acidic volcanic rocks, particularly for rhyolite and trachyte fallout ash beds. Albite ($NaAlSi_3O_8$) and sanidine form a continuous series of solid solutions, so their co-occurrence in the tonstein is quite appropriate and indicates a sufficient amount of sodium in the parent material. Anorthoclase ($(Na,K)AlSi_3O_8$) has an intermediate composition in the continuous series of sanidine and albite, and is characteristic of high-temperature (above 600 °C) sodium-rich volcanic rocks. Thus, its presence in tonstein is a direct indication of the pyroclastic nature and high alkalinity of the parent material.

The alkaline (pantellerite–comendite) composition of the primary ash material is also confirmed by the occurrence of low-stable complex zirconium–silicate minerals in association with leach-resistant zircons [38]. The presence of Zr-bearing minerals comprising zircon, baddeleyite, and complex Ca-Nb-Zr-P silicates of variable composition, along with the occurrence of lanthanides (monazite) and nodular sulphides (galena and sphalerite), suggests that the parent material, which was subsequently transformed into kaolinite and associated tonstein minerals, could have been derived from synchronous volcanic inputs (e.g., air-fall ash) [4,41,88,90,91]. Special geochemical studies have suggested that the most probable source of pantellerite ash for tonsteins from the XXX coal seam may be volcanic eruptions in Northern Mongolia [38].

Major elements of tonsteins determined by inductively coupled plasma atomic emission spectroscopy (ICP-AES). The tonsteins I-12 and I-22 are predominantly composed of SiO_2 and Al_2O_3, which in total exceed 50% (Table 2). The elevated SiO_2/Al_2O_3 ratio of 2.12 in tonstein I-12 is consistent with the increased silicification of the rock [38]. The lower SiO_2/Al_2O_3 value of 1.79 in tonstein I-22 is in agreement with the predominance of kaolinite in its composition.

The TiO_2/Al_2O_3 ratio (Table 2) is often used as an auxiliary criterion of the contribution of pyroclastics to coal accumulation [92] and for reconstructing the original composition of

altered ash material [41]. It is assumed that a value of the TiO_2/Al_2O_3 ratio below 0.02 is characteristic of rhyolitic pyroclastics [93].

The TiO_2/Al_2O_3 value for tonstein I-22 is 0.023, which may be evidence of the proximity of the original ash matter to rhyolitic pyroclastics [38]. A TiO_2/Al_2O_3 ratio between 0.02 and 0.06 indicates the contribution of intermediate or alkaline volcanic ash [93]. The TiO_2/Al_2O_3 value for tonstein I-12 is 0.036, which provides further confirmation that the parent matter was similar in composition to this type of volcanic ash.

Trace elements of tonsteins obtained by the ICP-MS method. The majority of trace elements in tonsteins I-12 and I-22 demonstrate comparable trends of change (increase or decrease) in concentrations compared to average contents (Table 3). Both tonsteins display an increase in most REEs (Sc, Y, and lanthanides). At the same time, the concentrations of some elements (e.g., Li, Be, Ni) exhibit multidirectional trends, with one tonstein showing an increase and the other a decrease compared to the average contents. A third group of elements, including La, Pr, Hf, Ta, and U, which have increased values in tonstein I-22, while in tonstein I-12 their contents are close to the average contents, is also distinguished. The differences in the content of chemical elements in the tonsteins can be attributed to the different composition of the parent volcanic ash [38].

Previous investigations of the studied tonsteins, in particular the analyses of the Eu anomaly and Zr/TiO_2-Nb/Y diagram [38], led to the conclusion of more acidic, rhyolite–pantellerite, parent pyroclastics in tonstein I-22 and more basic, dacite–rhyodacite, pyroclastics in tonstein I-12.

Zircons. The good preservation and idiomorphic crystallographic outlines of the majority (about 75%) of the zircon grains extracted from tonsteins I-22 and I-12 indicate that in both cases we are dealing with monomineral populations, each formed from a single magmatic melt. The dominance of subtypes S17, S18, and S19 of the main type S ({100}–{110}, {101}–{211}), the presence of long prismatic crystals of subtypes P4 ({100}>{110}) and P5 ({100}>>>{110}), and the grouping of morphotypes in the lower part of the J. P. Pupin's diagram of (Figures 14 and 15), confirm the homogeneity of the mineral populations and suggests similar conditions for the growth of most crystals in the temperature range 750–850 °C.

The crystallisation temperature of zircons from tonsteins I-22 and I-12 in the range 700–900 °C is confirmed by the analysis of melt inclusions. The small number of crystals with well-defined {110} facets crystallising at relatively lower temperatures is also consistent with this temperature range. There is evidence that, in addition to temperature, the growth medium has an influence on the morphology of zircons [94]; this suggestion requires further investigation.

These results are generally consistent with the general pattern of magmatic melt formation, where silica-rich acidic melts have a temperature range of 700–900 °C, whereas basic melts enriched in alkali and rare earth oxides have higher temperatures, typically above 900 °C [95,96]. Despite the fact that in both tonsteins the dominant morphotypes of zircon crystals are subtypes forming at 800°C, a trend of a slight increase in crystallisation temperature from the lower to the upper tonstein can be observed. Thus, tonstein I-22, which is thought to have formed from rhyolitic parent ash, includes six low-temperature morphotypes with crystallisation temperatures of 650–750 °C, whereas tonstein I-12, formed from intermediate or alkaline volcanic ash, contains only five low-temperature morphological subtypes, with crystallisation temperatures not lower than 700–750 °C.

In general, the petrography, mineral composition, and geochemical data of the tonsteins are in good agreement with the results of the morphological study of zircon crystals and the analysis of melt inclusions, indicating the formation of the parent ashes of the studied tonsteins and associated minerals from synchronous volcanic inputs (e.g., air-fall ash) derived from rhyolite–pantellerite (tonstein I-22) and dacite–rhyodacite (tonstein I-12) magmatic melts with temperatures of 700–900 °C.

Radioisotopic dating versus biostratigraphy. The radioisotopic weighted mean ages of 261.4 ± 0.7 Ma (MSWD = 2.7) (tonstein I-22) and 261.3 ± 0.4 Ma (MSWD = 0.5) (tonstein

I-12) (Figures 7 and 17) indicate that the host strata (coal seams XXX and XXXa; middle part of the Izykh Fm) belong to the Capitanian (Figure 2). At the same time, the biostratigraphic age of this interval is accepted nowadays as Roadian [44,59]. Thus, our dating suggests that the Izykh Fm is about 10 Ma younger than currently thought.

It should be noted that a direct correlation of the biostratigraphic data of the Minusinsk Basin with the subdivisions of the GSSR is impossible, because the Siberian palaeocontinent and the East European Platform with the Cis-Uralian Foredeep, the stratotype region of the GSSR stages, belong to different phytogeographic and zoogeographic provinces [32,97]. For this reason, the biostratigraphic age of the lithostratigraphic units of the Minusinsk Basin is determined by comparing their palaeontological and palaeobotanical assemblages with those of the Kuznetsk Basin, which serves as the adopted biostratigraphic standard [61,98]. Therefore, in Figure 2, the units of the Minusinsk Basin are correlated with the formations of the Kuznetsk Basin, and we will use these formations in further characterising the palaeobotanical features of the Izykh flora. It should be noted that the biostratigraphic units of the Kuznetsk Basin is conventionally correlated with the GSSR subdivisions and requiring constant refinement [30–32].

The rich collections of plant remains from the shale package overlying coal seam XXX were examined by Sivtchikov and Donova [44], who provided the list of taxa (unfortunately without illustration). According to the authors, this assemblage, which combines *Rufloria* and *Cordaites* with the upper surface of the leaves striated with numerous small furrows masking the veining, is characteristic of the Ilyinskoe Subgroup (Kazankovo-Markina and Uskat Fms) of the Kuznetsk Basin. In the approved Stratigraphic Scheme of the Kuzbass, the Ilyinskoe Subgroup is compared with the Kazanian Stage of the GSSR, which in turn is correlated with the Roadian Stage of the ICC [97,98].

In the opinion of L.G. Porokhovnichenko (this paper), the taxonomic composition of the assemblage reported by Sivtchikov and Donova [44] indicates that it belongs to the so-called Kolchugino flora in the time range of the Ilyinskoe Subgroup (Figure 2). This is supported by a number of taxa: *Tungussocarpus tychtensis* (appears only from the Ilyinskoe Subgroup of the Kuzbass and occurs in the interval including the Kazankovo–Markina Fm and Gramoteino Fm); *Tungussocarpus rotundatus* (Kazankovo–Markina Fm and Leninsk Fm); *Sylvella dubia* (Usa Beds and Erunakovo Subgroup); *Glottophyllum elongatum* (Kazankovo–Markina Fm and Leninsk Fm); *Rufloria brevifolia* (Kazankovo–Markina Fm and Uskat Fm); *Cordaites clercii* Zal. (uppermost Uskat Fm and Erunakovo Subgroup); *C. gorelovae* (Kuznetsk Subgroup and Leninsk Fm); and *C. gracilentus* (Kuznetsk Subgroup and lower Leninsk Fm).

Among the species mentioned above, only *Rufloria brevifolia* is limited to the Kazankovo–Markina and Uskat Fms (= Roadian). In contrast, the other species have more extensive stratigraphic ranges, which span the overlying Leninsk and Gramoteino Fm of the Erunakovo Subgroup (= Wordian–Capitanian). In addition, the list contains *Cordaites clercii*, a species occurring exclusively in the Erunakovo Subgroup. Assuming there was an error in the determination of *Rufloria brevifolia* (e.g., due to poor preservation of the specimen), the remaining floristic assemblage does not contradict the new radioisotopic dating.

The Upper Narylkova Subformation (Sfm) underlying the Izykh Fm is compared by floristic remains to the Ishanova and Kemerovo Fms of the Kuznetsk Basin (upper Balakhonka Subgroup = Artinskian–Kungurian) [44].

Plant remains of the Ishanova and Kemerovo Formations of the Kuznetsk Basin belong to the so-called Balakhonka flora, which, according to radioisotope data, ended its existence in the south of the Siberian palaeocontinent about 277 Ma [12]. The oldest plant assemblages of the Izykh Formation are similar to those of the Ilyinskoe Subgroup of the Kuznetsk Basin [25], which accumulated in the interval 273–266 Ma (Figure 2). Thus, new and already available radioisotope dating of the Minusinsk and Kuznetsk basins, compared with palaeobotanical data, indicate that the geological record of the Minusinsk Basin lacks strata corresponding approximately to the interval of 278–273 Ma (=Upper Kungurian) (Figure 2). The identified stratigraphic unconformity of about 5 Myr can be explained

by (1) either regional (or local) erosion of already accumulated strata, or (2) a hiatus in sediment accumulation.

The conclusion of a long hiatus in sedimentation is unusual for the geology of the coal-bearing upper Palaeozoic of Siberia. This succession, at least in the reference Kuznetsk Basin, is considered to be continuous, with only one distinct local unconformity at the boundary of the Balakhonka and Kolchugino Groups [51,99], and the temporal range of this gap is considered to be much shorter than the duration of the local stratons it separates.

Viktor Sivtchikov [44] was the first to note the significant role of unconformities in the coal-bearing sequence of the Minusinsk Basin, justifying the gap between the Izykh and Narylkova Fms and between the Narylkova and Beliy Yar Fms on the basis of palaeobotanical data, and suggesting the presence of a discontinuity within the Narylkova Fm. We agree with Sivtchikov (p. 23 in [44]) that insufficient attention of palaeontologists to the possible hiatus in the geological record of the Minusinsk Basin was expressed in their attempts to establish an uninterrupted sequence of fossil assemblages based on traditional ideas of continuous succession, which led to erroneous taxonomic definitions and incorrect interpretations of biostratigraphic age. New radioisotopic dating confirms Sivtchikov's observations [44] and reveals the necessity to review the available palaeontological data.

7. Conclusions

The petrography, structure, and mineralogical composition of the studied tonsteins confirm their origin from volcanic ashfalls. The results from X-ray diffraction analysis (XRD), energy-dispersive X-ray spectrometry (SEM-EDS), and inductively coupled plasma mass spectrometry (ICP-MS) establish the compositions of the parent pyroclastic materials as rhyolite–pantellerite for tonstein I-22 and more basic dacite–rhyodacite for tonstein I-12.

The morphological analysis of the zircon crystals, as well as the results of the cathodoluminescence and melt inclusion studies, confirm the unity of the mineral populations extracted from the tonsteins and the crystallisation of zircons from volcanic material at temperatures ranging from 700 to 900 °C.

New radioisotopic dates of 261.4 ± 0.7 Ma and 261.3 ± 0.4 Ma clarify the age of the Izykh Formation, enabling direct correlation of its upper part, including the XXX coal seam, with the Capitanian stage of the International Chronostratigraphic Chart.

The results highlight the possible discontinuity and incompleteness of the coal-bearing succession of the Siberian palaeocontinent, where gaps can span several million years.

The data demonstrate the potential for the radioisotopic dating of tonsteins, which are abundant in the coal-bearing strata of the Minusinsk Basin. Future work may provide new insights into the stratigraphic framework of coal seams and clarify the history of coal accumulation in the Siberian palaeocontinent during the Palaeozoic.

References

1. Schmitz, M.D.; Singer, B.S.; Rooney, A.D. Radioisotope Geochronology. In *Geologic Time Scale 2020*; Gradstein, F.M., Ogg, J.G., Schmitz, M.D., Ogg, G.M., Eds.; Elsevier: Amsterdam, The Netherlands, 2020; Volume 1, pp. 193–209. [CrossRef]
2. Wang, T.; Ramezani, J.; Yang, C.; Yang, J.; Wu, Q.; Zhang, Z.; Lv, D.; Wang, C. High-resolution geochronology of sedimentary strata by U-Pb CA-ID-TIMS zircon geochronology: A review. *Earth-Sci. Rev.* **2023**, *245*, 104550. [CrossRef]
3. Spears, D.A. A kaolinite mudstone (tonstein) in the British Coal Measures. *J. Sedim. Petrol.* **1970**, *40*, 386–394. [CrossRef]
4. Spears, D.A. The origin of tonsteins, an overview, and links with seatearths, fireclays and fragmental clay rocks. *Int. J. Coal Geol.* **2012**, *94*, 22–31. [CrossRef]
5. Spears, D.A.; Arbuzov, S.I. A geochemical and mineralogical update on two major tonsteins in the UK Carboniferous Coal Measures. *Int. J. Coal Geol.* **2019**, *210*, 103199. [CrossRef]
6. Lyons, P.C.; Spears, D.A.; Outerbridge, W.F.; Congdon, R.D.; Evans, H.T. Euramerican tonsteins: Overview, magmatic origin, and depositional-tectonic implications. *Palaeogeogr. Palaeoclimatol. Palaeoecol.* **1994**, *106*, 113–134. [CrossRef]
7. Opluštil, S.; Laurin, J.; Hýlová, L.; Jirásek, J.; Schmitz, M.; Sivek, M. Coal-bearing fluvial cycles of the late Paleozoic tropics; astronomical control on sediment supply constrained by high-precision radioisotopic ages, Upper Silesian Basin. *Earth-Sci. Rev.* **2022**, *228*, 103998. [CrossRef]
8. Shen, M.; Dai, S.; Graham, I.T.; Nechaev, V.P.; French, D.; Zhao, F.; Shao, L.; Liu, S.; Zuo, J.; Zhao, J.; et al. Mineralogical and geochemical characteristics of altered volcanic ashes (tonsteins and K-bentonites) from the latest Permian coal-bearing strata of western Guizhou Province, southwestern China. *Int. J. Coal Geol.* **2021**, *237*, 103707. [CrossRef]
9. Shen, M.; Dai, S.; Nechaev, V.P.; French, D.; Graham, I.T.; Liu, S.; Chekryzhov, I.Y.; Tarasenko, I.A.; Zhang, S. Provenance changes for mineral matter in the latest Permian coals from western Guizhou, southwestern China, relative to tectonic and volcanic activity in the Emeishan Large Igneous Province and Paleo-Tethys region. *Gondwana Res.* **2023**, *113*, 71–88. [CrossRef]
10. Lyons, P.C.; Krogh, T.E.; Kwok, Y.Y.; Davis, D.W.; Outerbridge, W.F.; Evans, H.T. Radiometric ages of the Fire Clay tonstein [Pennsylvanian (Upper Carboniferous), Westphalian, Duckmantian]: A comparison of U-Pb zircon single-crystal ages and 40Ar/39Ar sanidine single-crystal plateau ages. *Int. J. Coal Geol.* **2006**, *67*, 259–266. [CrossRef]
11. Ducassou, C.; Mercuzot, M.; Bourquin, S.; Rossignol, C.; Pellenard, P.; Beccaletto, L.; Poujol, M.; Hallot, E.; Pierson-Wickmann, A.C.; Hue, C.; et al. Sedimentology and U-Pb dating of Carboniferous to Permian continental series of the northern Massif Central (France): Local palaeogeographic evolution and larger scale correlations. *Palaeogeogr. Palaeoclimatol. Palaeoecol.* **2019**, *533*, 109228. [CrossRef]
12. Jirásek, J.; Opluštil, S.; Sivek, M.; Schmitz, M.D.; Abels, H.A. Astronomical forcing of Carboniferous paralic sedimentary cycles in the Upper Silesian Basin, Czech Republic (Serpukhovian, latest Mississippian): New radiometric ages afford an astronomical age model for European biozonations and substages. *Earth-Sci. Rev.* **2018**, *177*, 715–741. [CrossRef]
13. Opluštil, S.; Schmitz, M.; Cleal, C.J.; Martínek, K. A review of the Middle–Late Pennsylvanian west European regional substages and floral biozones, and their correlation to the Geological Time Scale based on new U–Pb ages. *Earth-Sci. Rev.* **2016**, *154*, 301–335. [CrossRef]
14. Pellenard, P.; Gand, G.; Schmitz, M.; Galtier, J.; Broutin, J.; Stéyer, J.S. High-precision U-Pb zircon ages for explosive volcanism calibrating the NW European continental Autunian stratotype. *Gondwana Res.* **2017**, *51*, 118–136. [CrossRef]
15. Davydov, V.I.; Crowley, J.L.; Schmitz, M.D.; Poletaev, V.I. High-Precision U-Pb Zircon Age Calibration of the Global Carboniferous Time Scale and Milankovitch Band Cyclicity in the Donets Basin, Eastern Ukraine. *Geochem. Geophys. Geosystems* **2010**, *11*, Q0AA04. [CrossRef]
16. Davydov, V.I.; Korn, D.; Schmitz, M.D. The Carboniferous period. In *The Geologic Time Scale*, 1st ed.; Gradstein, F.M., Ogg, J.G., Schmitz, M., Ogg, G., Eds.; Elsevier: Oxford, UK, 2012; pp. 603–651. [CrossRef]
17. Metcalfe, I.; Crowley, J.L.; Nicoll, R.S.; Schmitz, M. High-precision U-Pb CA-TIMS calibration of Middle Permian to Lower Triassic sequences, mass extinction and extreme climate-change in eastern Australian Gondwana. *Gondwana Res.* **2015**, *28*, 61–81. [CrossRef]
18. Shi, G.R.; Nutman, A.P.; Lee, S.; Jones, B.G.; Bann, G.R. Reassessing the chronostratigraphy and tempo of climate change in the Lower-Middle Permian of the southern Sydney Basin, Australia: Integrating evidence from U–Pb zircon geochronology and biostratigraphy. *Lithos* **2022**, *410–411*, 106570. [CrossRef]
19. Sobczak, K.; Cooling, J.; Crossingham, T.; Holl, H.G.; Reilly, M.; Esterle, J.; Crowley, J.L.; Hannaford, C.; Mohr, M.T.; Hamerli, Z.; et al. Palynostratigraphy and Bayesian age stratigraphic model of new CA-ID-TIMS zircon ages from the Walloon Coal Measures, Surat Basin, Australia. *Gondwana Res.* **2024**, *132*, 150–167. [CrossRef]
20. Cagliari, J.; Schmitz, M.D.; Tedesco, J.; Trentin, F.A.; Lavina, E.L.C. High-precision U-Pb geochronology and Bayesian age-depth modelling of the glacial-postglacial transition of the southern Paraná Basin: Detailing the terminal phase of the Late Paleozoic Ice Age on Gondwana. *Sediment. Geol.* **2023**, *451*, 106397. [CrossRef]
21. Cagliari, J.; Lavina, E.L.C.; Philipp, R.P.; Tognoli, F.M.W.; Basei, M.A.S.; Faccini, U.F. New Sakmarian ages for the Rio Bonito formation (Paraná Basin, southern Brazil) based on LA-ICP-MS U-Pb radiometric dating of zircons crystals. *J. S. Am. Earth Sci.* **2014**, *56*, 265–277. [CrossRef]
22. Guerra-Sommer, M.; Cazzulo-Klepzig, M.; Santos, J.O.S.; Hartmann, L.A.; Ketzer, J.M.; Formoso, M.L.L. Radiometric age determination of tonsteins and stratigraphic constraints for the Lower Permian coal succession in southern Paraná Basin, Brazil. *Int. J. Coal Geol.* **2008**, *74*, 13–27. [CrossRef]

23. Jurigan, I.; Ricardi-Branco, F.; Neregato, R.; dos Santos, T.J.S. A new tonstein occurrence in the eastern Paraná Basin associated with the Figueira coalfield (Paraná, Brazil): Palynostratigraphy and U-Pb radiometric dating integration. *J. S. Am. Earth Sci.* **2019**, *96*, 102377. [CrossRef]

24. Mori, A.L.O.; de Souza, P.A.; Marques, J.C.; da Cunha Lopes, R. A new U-Pb zircon age dating and palynological data from a Lower Permian section of the southernmost Paraná Basin, Brazil: Biochronostratigraphical and geochronological implications for Gondwanan correlations. *Gondwana Res.* **2012**, *21*, 654–669. [CrossRef]

25. Simas, M.W.; Guerra-Sommer, M.; Cazzulo-Klepzig, M.; Menegat, R.; Schneider Santos, J.O.; Fonseca Ferreira, J.A.; Degani-Schmidt, I. Geochronological correlation of the main coal interval in Brazilian Lower Permian: Radiometric dating of tonstein and calibration of biostratigraphic framework. *J. S. Am. Earth Sci.* **2012**, *39*, 1–15. [CrossRef]

26. Feng, Y.; Yang, T.; Liang, F.; Liu, F.; Sun, G. New zircon U–Pb age of the Didao Formation in Jixi Basin and its significance for the geology and paleogeography in Jixi and eastern Heilongjiang region in the Early Cretaceous. *Cretac. Res.* **2022**, *135*, 105169. [CrossRef]

27. Wang, J.; Shao, L.Y.; Wang, H.; Spiro, B.; Large, D. SHRIMP zircon U–Pb ages from coal beds across the Permian–Triassic boundary, eastern Yunnan, southwestern China. *J. Palaeogeogr.* **2018**, *7*, 117–129. [CrossRef]

28. Zhang, Z.; Lv, D.; Hower, J.C.; Wang, L.; Shen, Y.; Zhang, A.; Xu, J.; Gao, J. Geochronology, mineralogy, and geochemistry of tonsteins from the Pennsylvanian Taiyuan Formation of the Jungar Coalfield, Ordos Basin, North China. *Int. J. Coal Geol.* **2023**, *267*, 104183. [CrossRef]

29. Mikheeva, E.A.; Demonterova, E.I.; Khubanov, V.B.; Ivanov, A.V.; Arzhannikova, A.V.; Arzhannikov, S.G.; Blinov, A.V. Age of the coal accumulation in the irkutsk basin based on accessory zircon dating in the azeisk deposit tonstein (LA-ICP-MS). *Vestn. St. Petersburg Univ. Earth Sci.* **2020**, *65*, 420–433. [CrossRef]

30. Davydov, V.I.; Karasev, E.V.; Nurgalieva, N.G.; Schmitz, M.D.; Budnikov, I.V.; Biakov, A.S.; Kuzina, D.M.; Silantiev, V.V.; Urazaeva, M.N.; Zharinova, V.V.; et al. Climate and biotic evolution during the Permian-Triassic transition in the temperate Northern Hemisphere, Kuznetsk Basin, Siberia, Russia. *Palaeogeogr. Palaeoclimatol. Palaeoecol.* **2021**, *573*, 110432. [CrossRef]

31. Silantiev, V.V.; Gutak, Y.M.; Tichomirowa, M.; Kulikova, A.V.; Felker, A.S.; Urazaeva, M.N.; Porokhovnichenko, L.G.; Karasev, E.V.; Bakaev, A.S.; Zharinova, V.V.; et al. First radiometric dating of tonsteins from coal-bearing succession of the Kuznetsk Basin: U-Pb geochronology of the Tailugan Formation. *Georesursy=Georesources* **2023**, *25*, 203–227. [CrossRef]

32. Silantiev, V.V.; Gutak, Y.M.; Tichomirowa, M.; Käßner, A.; Kutygin, R.V.; Porokhovnichenko, L.G.; Karasev, E.V.; Felker, A.S.; Bakaev, A.S.; Naumcheva, M.A.; et al. U-Pb Dating of the Kolchugino Group Basement (Kuznetsk Coal Basin, Siberia): Was the Change in Early–Middle Permian Floras Simultaneous at Different Latitudes in Angaraland? *Geosciences* **2024**, *14*, 21. [CrossRef]

33. Admakin, L.A. Types of tonsteins in coal beds of Minusinsk basin. *Lithol. Min. Res.* **1992**, *2*, 49–56. (In Russian)

34. Arbuzov, S.I.; Ershov, V.V.; Rikhvanov, L.P.; Kyargin, V.V.; Bulatov, A.A.; Dubovik, P.E. *Rare-Metal Potential of Coals of Minusinsk Basin*; Publishing House SO RAN Branch "GEO": Novosibirsk, Russia, 2003; 347p. (In Russian)

35. Arbuzov, S.I.; Ilenok, S.S.; Vergunov, A.V.; Shaldybin, M.V.; Sobolenko, V.M.; Nekrasov, P.E. Mineralogical-geochemical identification of explosive volcanism products in coals of the Minusinsk basin. In *Petrology of Magmatic and Metamorphic Complexes. Issue 9, Proceedings of 9th All-Russian Petrographic Conference*; CSTI: Tomsk, Russia, 2017; pp. 35–37. (In Russian)

36. Vergunov, A.V.; Arbuzov, S.I.; Sobolenko, V.M. Mineralogy and geochemistry of the tonsteins in the coals of the Beisk deposit of Minusinsk Basin. Bull. Tomsk Polytech. *Univ. Geo Assets Eng.* **2019**, *330*, 155–166. (In Russian with English Abstract) [CrossRef]

37. Vergunov, A.V.; Arbuzov, S.I.; Eremeyeva, V.V. Mineralogy, geochemistry and genesis of rare-metal Zr-Nb-Hf-Ta-REE-Ga mineralization in bed XXX of Minusinsk Basin. *Bull. Tomsk Polytech. Univ. Geo Assets Eng.* **2020**, *331*, 49–62. (In Russian with English Abstract) [CrossRef]

38. Vergunov, A.V.; Arbuzov, S.I.; Spears, D.A.; Kholodov, A.S.; Ilenok, S.S. Mineralogy and geochemistry of rare metal (Zr-Nb-Hf-Ta-REE-Ga) coals of the seam XXX of the Izykh Coalfield, Minusinsk Basin, Russia: Implications for more widespread rare metal mineralization in North Asia. *Int. J. Coal Geol.* **2024**, *289*, 104542. [CrossRef]

39. Hower, J.C.; Rupport, L.F.; Cortland, F.E. Lanthanide, yttrium, and zirconium anomalies in the Fire Clay coal bed, Eastern Kentucky. *Int. J. Coal Geol.* **1999**, *39*, 141–153. [CrossRef]

40. Dai, S.; Zhou, Y.; Zhang, M.; Wan, G.X.; Wang, J.; Song, X.; Jiang, Y.; Luo, Y.; Song, Z.; Yang, Z.; et al. A new type of Nb (Ta)-Zr(Hf)-REE-Ga polymetallic deposit in the late Permian coal-bearing strata, eastern Yunnan, southwestern China: Possible economic significance and genetic implications. *Int. J. Coal Geol.* **2010**, *83*, 55–63. [CrossRef]

41. Dai, S.; Ward, C.R.; Graham, I.T.; French, D.; Hower, J.C.; Zhao, L.; Wang, X. Altered volcanic ashes in coal and coal-bearing sequences: A review of their nature and significance. *Earth-Sci. Rev.* **2017**, *175*, 44–74. [CrossRef]

42. Dai, S.; Nechaev, V.P.; Chekryzhov, I.Y.; Zhao, L.; Vysotskiy, S.V.; Graham, I.; Ward, C.R.; Ignatiev, A.V.; Velivetskaya, T.A.; Zhao, L. A model for Nb–Zr–REE–Ga enrichment in Lopingian altered alkaline volcanic ashes: Key evidence of H-O isotopes. *Lithos* **2018**, *302–303*, 359–369. [CrossRef]

43. Arbuzov, S.I.; Spears, D.A.; Vergunov, A.V.; Ilenok, S.S.; Mezhibor, A.M.; Ivanov, V.P.; Zarubina, N.A. Geochemistry, mineralogy and genesis of rare metal (Nb-Ta-Zr-Hf-Y-REE-Ga) coals of the seam XI in the south of Kuznetsk Basin, Russia. *Ore Geol. Rev.* **2019**, *113*, 103073. [CrossRef]

44. Sivtchikov, V.E.; Donova, N.B. Stratigraphic subdivision of the Upper Palaeozoic deposits of the South Minusinsk Depression. *Lethaea Ross. Russ. Palaeobot. J.* **2016**, *13*, 1–46.

45. Neiburg, M.F. Stratigraphic comparison of coal-bearing strata of the Minusinsk and Kuznetsk basins in Siberia. In *Proceedings Devoted to Academician V.I. Obruchev*; Publishing House of the USSR Academy of Sciences: Moscow, Russia, 1938; Volume 1, pp. 27–40. (In Russian)

46. Radchenko, G.P. Guiding forms of the Upper Paleozoic flora of the Altai-Sayan region. In *Atlas of Guiding Forms of Fossil Flora and Fauna of Western Siberia, Part II*; Khalfin, L.L., Ed.; Gosgeoltekhizdat: Moscow, Russia, 1955; pp. 42–154. (In Russian)

47. Spasskaya, I.S. On the assemblages of bivalve molluscs of coal-bearing strata of the Izykh field in the Minusinsk coal basin. In *Continental Upper Paleozoic and Mesozoic of Siberia and Central Kazakhstan: Biostratigraphy and Palaeontology*; Nalivkin, D.V., Ed.; Nauka: Moscow-Leningrad, Russia, 1966; pp. 5–40. (In Russian)

48. Gorelova, S.G. Phytostratigraphic characterisation of coal-bearing strata of the Minusinsk basin. In *Coal-Bearing Strata of the Kuznetsk and Tunguska Provinces*; Zvonarev, I.N., Ed.; Proceedings of the SNIIGGiMS, 221; SNIIGGiMS: Novosibirsk, Russia, 1975; pp. 47–56. (In Russian)

49. Dryagina, L.L. Palynological assemblages of coal seams of the Izykh deposit of the Minusinsk basin. In *Coal-Bearing Strata of the Kuznetsk and Tunguska Provinces*; Zvonarev, I.N., Ed.; Proceedings of the SNIIGGiMS, 221; SNIIGGiMS: Novosibirsk, Russia, 1975; pp. 57–58. (In Russian)

50. Troshkova, G.N.; Zhichko, L.A. Coal-bearing strata of the Minusinsk basin. In *Stratigraphy of the Palaeozoic of Middle Siberia*; Sokolov, B.S., Ed.; Nauka: Novosibirsk, Russia, 1967; pp. 186–189. (In Russian)

51. Betekhtina, O.A.; Gorelova, S.G.; Dryagina, L.L.; Danilov, V.I.; Batyaeva, S.P.; Tokareva, P.A. *Upper Paleozoic of Angarida*; Zhuravleva, I.T., Ilyina, V.I., Eds.; Nauka: Novosibirsk, Russia, 1988; 265p. (In Russian)

52. Fedotova, V.A.; Fedotov, A.N. Minusinsk Coal Basin. General information. Geological overview. Coal-bearing capacity. In *Coal Base of Russia. Coal Basins and Deposits of Eastern Siberia*; Cherepovsky, V.F., Ed.; LLC "Geoinformcentre": Moscow, Russia, 2002; Volume 3, pp. 173–201. (In Russian)

53. Buslov, M.M.; Geng, H.; Travin, A.V.; Otgonbaatar, D.; Kulikova, A.V.; Chen, M.; Stijn, G.; Semakov, N.N.; Rubanova, E.S.; Abildaeva, M.A.; et al. Tectonics and geodynamics of Gorny Altai and adjacent structures of the Altai–Sayan folded area. *Russ. Geol. Geophys.* **2013**, *54*, 1250–1271. [CrossRef]

54. Parfenov, L.M.; Khanchuk, A.I.; Badarch, G.; Miller, R.J.; Naumova, V.V.; Nokleberg, W.J.; Ogasawara, M.; Prokopiev, V.; Yan, H. *Geodynamics Map of Northeast Asia*; Scientific Investigations Map 3024. Scale 1:5 000 000; 2 sheets; U.S. Geological Survey: Reston, VA, USA, 2013. [CrossRef]

55. Tectonic Map of Northern-Central-Eastern Asia and Adjacent Areas; Scale 1:2 500 000. In *Atlas of Geological Maps of Northern-Central-Eastern Asia and Adjacent Areas*; Petrov, O.V.; Leonov, Y.G.; Tingdong, L.; Tomurtogoo, O. (Eds.) VSEGEI Publishing House: St. Petersburg, Russia, 2014. Available online: https://karpinskyinstitute.ru/ru/info/inter-proj/tect-asia2500/ (accessed on 23 August 2024).

56. Petrov, O.V.; Khanchuk, A.I.; Shokalsky, S.P.; Babin, G.A.; Pospelov, I.I. Principles of tectonic mapping of Asia and the Arctic, scales 1:2 500 000–1:5 000 000. *Geodyn. Tectonophys.* **2021**, *12*, 173–198. [CrossRef]

57. Gusev, G.S.; Mezhelovskiy, N.V.; Morozov, A.F.; Kilipko, V.A.; Sirotkina, O.N. Ob-Zaisan, Altai-Sayan and East Sayan-Yenisei orogens: Major features of tectonic development. *Reg. Geol. Metallog.* **2017**, *72*, 26–41. (In Russian)

58. Zhimulev, F.I.; Pospeeva, E.V.; Novikov, I.S.; Potapov, V.V. Deep structure of the Salair fold-nappe terrane (NW CAOB) according to magnetotelluric sounding. *Geodyn. Tectonophys.* **2021**, *12*, 125–138. [CrossRef]

59. Fedotov, A.N.; Ladygin, S.V.; Izmailova, S.A.; Sivtchikov, V.E.; Kalinin, V.V.; Izmaylova, S.A.; Kalinin, V.A.; Tsareva, E.V.; Lysogorsky, K.V.; Kacheev, Y.F. *State Geological Map of Russian Federation; Scale 1:200 000*, 2nd ed.; Minusinsk series. Sheet N-46-XX (Abakan). Explanatory note [Electronic resource]; Moscow branch of FSBI "VSEGEI": Moscow, Russia, 2019; 78p. Available online: https://www.geokniga.org/maps/31048 (accessed on 27 September 2024). (In Russian)

60. *Decisions of the All-Union Conference on the Development of Unified Stratigraphic Schemes for the Precambrian, Paleozoic and Quaternary Systems of Central Siberia (Novosibirsk, 1979). Part 2 (Middle and Upper Paleozoic)*; SRIGGMRM: Novosibirsk, Russia, 1982; 129p. (In Russian)

61. Budnikov, I.V. (Ed.) Decision of the Meeting on the stratigraphy of the Upper Paleozoic deposits of Kuzbass. In *Kuznetsk Basin—Key Region in Stratigraphy of the Angarida Upper Paleozoic*; YuzhSibgeolkom: Novosibirsk, Russia, 1996; Volume 2, pp. 93–94. (In Russian)

62. Zhamoida, A.I. (Ed.) *Stratigraphic Guide of Russia*, 3rd ed.; Corrected and supplemented; VSEGEI: St. Petersburg, Russia, 2019; 96p. (In Russian)

63. International Chronostratigraphic Chart. Available online: https://stratigraphy.org/ICSchart/ChronostratChart2023-06.pdf (accessed on 7 July 2024).

64. Davydov, V.I.; Arefiev, M.P.; Golubev, V.K.; Karasev, E.V.; Naumcheva, M.A.; Schmitz, M.D.; Silantiev, V.V.; Zharinova, V.V. Radioisotopic and biostratigraphic constraints on the classical Middle–Upper Permian succession and tetrapod fauna of the Moscow syneclise, Russia. *Geology* **2020**, *48*, 742–747. [CrossRef]

65. Bezzubtsev, V.V.; Perfilova, O.Y. *State Geological Map of Russian Federation; Scale 1: 1 000 000*; Third generation. Series Altai-Sayan. Sheet N-46 (Abakan); Cartographic factory "VSEGEI": St. Petersburg, Russia, 2008; 391p. Available online: https://www.geokniga.org/sites/geokniga/files/mapcomments/n-46-abakan-gosudarstvennaya-geologicheskaya-karta-rossiyskoy-federacii-tre.pdf (accessed on 27 September 2024). (In Russian)

66. Moore, D.M.; Reynoldsl, R.C., Jr. *X-ray Diffraction and the Identification and Analysis of Clay Minerals*; Oxford University Press: Oxford, UK, 1997; 400p.
67. Taylor, J.C. Computer programs for standardless quantitative analysis of minerals using the full powder diffraction profile. *Powder Diffract.* **1991**, *6*, 2–9. [CrossRef]
68. Bish, D.L.; Post, J.E. Quantitative mineralogical analysis using the Rietveld fullpattern fitting method. *Am. Min.* **1993**, *78*, 932–940.
69. Markl, G. *Minerale und Gesteine. Mineralogie–Petrologie–Geochemie*, 2nd ed.; Spectrum Akademischer Verlag: Heidelberg, Germany, 2008; 61p. (In German)
70. Pupin, J.P. Zircon and granite petrology. *Contrib. Mineral. Petrol.* **1980**, *73*, 207–220. [CrossRef]
71. Mattinson, J.M. Zircon U-Pb chemical abrasion ("CA-TIMS") method: Combined annealing and multi-step partial dissolution analysis for improved precision and accuracy of zircon ages. *Chem. Geol.* **2005**, *220*, 47–66. [CrossRef]
72. Condon, D.J.; Schoene, B.; McLean, N.M.; Bowring, S.A.; Parrish, R.R. Metrology and traceability of U–Pb isotope dilution geochronology (EARTHTIME Tracer Calibration Part I). *Geochim. Cosmochim. Acta* **2015**, *164*, 464–480. [CrossRef]
73. Gerstenberger, H.; Haase, G. A highly effective emitter substance for mass spectrometric Pb isotope ratio determinations. *Chem. Geol.* **1997**, *136*, 309–312. [CrossRef]
74. Wiedenbeck, M.; Alle, P.; Corfu, F.; Griffin, W.L.; Meier, M.; Oberli, F.; Von Quadt, A.; Roddick, J.C.; Spiegel, W. Three Natural Zircon Standards for U-Th-Pb, Lu-Hf, Trace Element and Ree Analyses. *Geostand. Newsl.* **1995**, *19*, 1–23. [CrossRef]
75. Black, L.P.; Kamo, S.L.; Allen, C.M.; Davis, D.W.; Aleinikoff, J.N.; Valley, J.W.; Mundil, R.; Campbell, I.H.; Korsch, R.J.; Williams, I.S.; et al. Improved $^{206}Pb/^{238}U$ microprobe geochronology by the monitoring of a trace-element related matrix effect; SHRIMP, ID-TIMS, ELA-ICP-MS and oxygen isotope documentation for a series of zircon standards. *Chem. Geol.* **2004**, *205*, 115–140. [CrossRef]
76. Schaltegger, U.; Ovtcharova, M.; Gaynor, S.; Schoene, B.; Wotzlaw, J.-F.; Davies, J.; Farina, F.; Greber, N.D.; Szymanowski, D.; Chelle-Michou, C. Long-term repeatability and interlaboratory reproducibility of high-precision ID-TIMS U-Pb geochronology. *J. Anal. At. Spectrom.* **2021**, *36*, 1466–1477. [CrossRef]
77. Schoene, B.; Crowley, J.L.; Condon, D.C.; Schmitz, M.D.; Bowring, S.A. Reassessing the uranium decay constants for geochronology using ID-TIMS U–Pb data. *Geochim. Cosmochim. Acta* **2006**, *70*, 426–445. [CrossRef]
78. Rudnick, R.L.; Gao, S. Composition of the continental crust. In *Treatise on Geochemistry*; Holland, H.D., Turekian, K.K., Eds.; Elsevier: Amsterdam, The Netherlands, 2014; Volume 3, pp. 1–64. [CrossRef]
79. Gromet, L.P.; Haskin, L.A.; Korotev, R.L.; Dymek, R.F. The "North American shale composite": Its compilation, major and trace element characteristics. *Geochim. Cosmochim. Acta* **1984**, *48*, 2469–2482. [CrossRef]
80. Grigoryev, N.A. About chemical elements Clark content in the upper part of continental crust. *Litosphera [Lithosphere]* **2002**, *1*, 61–71. (In Russian)
81. Grigorev, N.A. Average concentrations of chemical elements in rocks of the upper continental crust. *Geochem. Int.* **2003**, *41*, 711–718.
82. Ketris, M.P.; Yudovich, Y.E. Estimations of Clarkes for Carbonaceous biolithes: World averages for trace element contents in black shales and coals. *Int. J. Coal Geol.* **2009**, *78*, 135–148. [CrossRef]
83. Bowring, J.F.; McLean, N.M.; Bowring, S.A. Engineering cyber infrastructure for U-Pb geochronology: Tripoli and U-Pb_Redux. *Geochem. Geophys. Geosystems* **2011**, *12*, Q0AA19. [CrossRef]
84. Zaritsky, P.V. Origin of tonsteins within Donbass coal seams. *Rep. USSR Acad. Sci.* **1967**, *177*, 422–425.
85. Zaritsky, P.V. A review of the study of tonsteins in the Donetz basin. In *Congres International de Stratigraphie et Geologie du Carbonifere, 10th, Madrid, 1983, Comptes Rendus*; Inst. Geologico y Mineiro de España: Madrid, Spain, 1985; Volume 4, pp. 235–241.
86. Loughnan, F.C. Flint clays, tonsteins and the kaolinite clayrock facies. *Clay Miner.* **1978**, *13*, 387–400. [CrossRef]
87. Chernovyants, M.G. *Tonsteins and Their Use in the Study of Coalbearing Formations*; Nedra: Moscow, Russia, 1992; 144p. (In Russian)
88. Bohor, B.F.; Triplehorn, D.M. Tonsteins: Altered Volcanic-Ash Layers in Coal-Bearing Sequences. In *Geological Society of America Special Papers*; Geological Society of America: Boulder, CO, USA, 1993; Volume 285, pp. 1–44. [CrossRef]
89. Demchuk, T.D.; Nelson-Glatiotis, D.A. The identification and significance of kaolinite-rich, volcanic ash horizons (tonsteins) in the Ardley coal zone, Wabamun, Alberta, Canada. *Bull. Can. Pet. Geol.* **1993**, *41*, 464–469. [CrossRef]
90. Burger, K.; Bandelow, F.K.; Bieg, G. Pyroclastic kaolin coal–tonsteins of the Upper Carboniferous of Zonguldak and Amasra. *Turkey. Int. J. Coal Geol.* **2000**, *45*, 39–53. [CrossRef]
91. Arbuzov, S.I.; Mezhibor, A.M.; Spears, D.A.; Ilenok, S.S.; Shaldybin, M.V.; Belaya, E.V. Nature of tonsteins in the Azeisk deposit of the Irkutsk Coal Basin (Siberia, Russia). *Int. J. Coal Geol.* **2016**, *153*, 99–111. [CrossRef]
92. Yudovich, Y.E.; Ketris, M.P. Fundamentals of Lithochemistry. Nauka: St. Petersburg, Russia, 2000; 479p. (In Russian)
93. Spears, D.A.; Kanaris-Sotiriou, R. A geochemical and mineralogical investigation of some British and other European tonsteins. *Sedimentology* **1979**, *26*, 407–425. [CrossRef]
94. Benisek, A.; Finger, F. Factors controlling the development of prism faces in granite zircons: A microprobe study. *Contrib. Mineral. Petrol.* **1993**, *114*, 441–451. [CrossRef]
95. Ghiorso, M.S.; Sack, R.O. Chemical mass transfer in magmatic processes IV. A revised and internally consistent thermodynamic model for the interpolation and extrapolation of liquid-solid equilibria in magmatic systems at elevated temperatures and pressures. *Contrib. Mineral. Petrol.* **1995**, *119*, 197–212. [CrossRef]

96. Annen, C.; Zellmer, G.F. *Dynamics of Crustal Magma Transfer, Storage and Differentiation*; Geological Society:Special Publications: London, UK, 2008; Volume 304, pp. 35–59. [CrossRef]
97. Schneider, J.W.; Lucas, S.G.; Scholze, F.; Voigt, S.; Marchetti, L.; Klein, H.; Opluštil, S.; Werneburg, R.; Golubev, V.K.; Barrick, J.E.; et al. Late Paleozoic–early Mesozoic continental biostratigraphy—Links to the Standard Global Chronostratigraphic Scale. *Palaeoworld* **2020**, *29*, 186–238. [CrossRef]
98. Budnikov, I.V.; Kutygin, R.V.; Shi, G.R.; Sivtchikov, V.E.; Krivenko, O.V. Permian stratigraphy and paleogeography of Central Siberia (Angaraland)—A review. *J. Asian Earth Sci.* **2020**, *196*, 104365. [CrossRef]
99. Gorelova, S.G.; Budnikov, I.V. Main stages of studying the stratigraphy of the Upper Palaeozoic of Kuzbass. In *Kuznetsk Basin—Key Region in Stratigraphy of the Angarida Upper Paleozoic*; Budnikov, I.V., Ed.; YuzhSibgeolkom: Novosibirsk, Russia, 1996; Volume 1, pp. 7–12. (In Russian)